
ForkMerge: Overcoming Negative Transfer in Multi-Task Learning

Junguang Jiang^{1*} Baixu Chen^{1*} Junwei Pan² Ximei Wang² Liu Dapeng² Jie Jiang² Mingsheng Long¹

Abstract

The goal of multi-task learning is to utilize useful knowledge from multiple related tasks to improve the generalization performance of all tasks. However, learning multiple tasks simultaneously often results in worse performance than learning them independently, which is known as negative transfer. Most previous works attribute negative transfer in multi-task learning to gradient conflicts between different tasks and propose several heuristics to manipulate the task gradients for mitigating this problem, which mainly considers the optimization difficulty and overlooks the generalization problem. To fully understand the root cause of negative transfer, we experimentally analyze negative transfer from the perspectives of optimization, generalization, and hypothesis space. Stemming from our analysis, we introduce *ForkMerge*, which periodically forks the model into multiple branches with different task weights, and merges dynamically to filter out detrimental parameter updates to avoid negative transfer. On a series of multi-task learning tasks, *ForkMerge* achieves improved performance over state-of-the-art methods and largely avoids negative transfer.

1. Introduction

Multi-Task Learning (MTL) (Caruana, 1997) is expected to improve learning efficiency and prediction accuracy by learning multiple objectives from a shared representation. It is shown to improve generalization in theory (Baxter, 2000) and has been prevalent in many machine learning applications, such as computer vision (Silberman et al., 2012), natural language understanding (Liu et al., 2019c), computational advertising (Li et al., 2020), computational chemistry (Ramakrishnan et al., 2014), and robotics (Yu et al., 2020b).

However, in practice, learning multiple tasks simultaneously often leads to performance degradation compared to learn-

ing tasks individually, a phenomenon known as *negative transfer* (Zhang et al., 2022). There has been a significant amount of methods proposed to mitigate negative transfer in MTL (Liu et al., 2019b; Yu et al., 2020a; Liu et al., 2021a; Javaloy & Valera, 2022). Notable previous works attribute negative transfer to the optimization difficulty, especially the gradient conflicts between different tasks (Yu et al., 2020a; Javaloy & Valera, 2022) and propose to overcome negative transfer by avoiding undesirable interference between task gradients (Liu et al., 2021a; Wang et al., 2021) or balancing gradient magnitudes (Chen et al., 2018b). Even though, the problem of negative transfer is still not well understood.

In this regard, we experimentally analyze the potential causes of negative transfer in MTL from three perspectives: optimization, generalization, and hypothesis space. From an optimization view, our experiments suggest that *gradient conflicts do not necessarily lead to negative transfer*. A perfect example is weight decay, which is very likely to conflict with the target task in gradients but still beneficial to the target performance. Further, in terms of generalization, we observe that negative transfer is more likely to occur when *the distribution shift between the multi-task training data and target test data is enlarged*. Lastly, we find that negative transfer is also likely to occur when *the distance from the learned hypothesis to the optimal hypothesis is increased*, which also inspires a new way to reduce negative transfer by decreasing the distance to the optimal hypothesis.

Based on our above analysis and findings, we present a new approach named *ForkMerge*. Specifically, we first fork the model into multiple branches with the same initialization. Then the parameters of different branches will be optimized on diverse data distributions which are constructed by varying the task weights of different branches. Finally, at regular intervals, we will merge and synchronize the parameters of each branch, in which way we will filter out harmful parameter updates to avoid negative transfer and keep desirable parameter updates to promote positive transfer.

The contributions of this work are summarized as follows: (1) We systematically identify the problem and analyze the causes of negative transfer in MTL. (2) We propose *ForkMerge*, a novel approach to mitigate negative transfer and boost the performance of MTL. (3) We conduct extensive experiments and validate that *ForkMerge* outperforms pre-

*Equal contribution ¹School of Software, BNRist, Tsinghua University, China ²Tencent Inc, China. Correspondence to: Mingsheng Long <mingsheng@tsinghua.edu.cn>.

vious methods on a series of MTL benchmarks, covering computer vision, recommender system, and molecule tasks.

2. Negative Transfer Analysis in MTL

Problem and Notation. MTL aims to find parameters θ of a model h_θ that achieve higher average performance on multiple tasks. Formally, given K different tasks denoted as $\{\mathcal{T}_j\}_{j=1}^K$, we optimize the model with

$$\min_{\theta} \sum_{j=1}^K [\lambda_j \mathbb{E}_{(\mathbf{x}, y) \sim \mathcal{T}_j} \mathcal{L}_j(\mathbf{x}, y; \theta)], \quad (1)$$

where \mathcal{L}_j is the training loss for task \mathcal{T}_j and λ_j is a task-weighting hyper-parameter. Our final objective is: $\max_{\theta} \sum_{j=1}^K [\mathcal{P}_j(\theta)]$ where \mathcal{P}_j is the relative performance measure for task \mathcal{T}_j , such as the accuracy in classification, which indicates better performance when the value is higher.

For simplicity of analysis, in this section, we mainly consider the case of one auxiliary task \mathcal{T}_{aux} and one target task \mathcal{T}_{tgt} . Then the optimization objective is reduced to

$$\min_{\theta} \mathbb{E}_{\mathcal{T}_{\text{tgt}}} \mathcal{L}_{\text{tgt}}(\theta) + \lambda \mathbb{E}_{\mathcal{T}_{\text{aux}}} \mathcal{L}_{\text{aux}}(\theta), \quad (2)$$

where λ is the relative weighting hyper-parameter between the auxiliary task and the target task. Next we define the Transfer Gain to measure the impact of \mathcal{T}_{aux} on \mathcal{T}_{tgt} .

Definition 2.1 (Transfer Gain, TG). Denote the model obtained by some MTL algorithm \mathcal{A} as $\theta_{\mathcal{A}}(\mathcal{T}_{\text{tgt}}, \mathcal{T}_{\text{aux}}, \lambda)$ and the model obtained by single-task learning on target task as $\theta_{\mathcal{A}}(\mathcal{T}_{\text{tgt}})$. Let \mathcal{P} be a performance measure on the target task \mathcal{T}_{tgt} . Then the algorithm \mathcal{A} can be evaluated by:

$$TG(\lambda, \mathcal{A}) = \mathcal{P}(\theta_{\mathcal{A}}(\mathcal{T}_{\text{tgt}}, \mathcal{T}_{\text{aux}}, \lambda)) - \mathcal{P}(\theta_{\mathcal{A}}(\mathcal{T}_{\text{tgt}})). \quad (3)$$

Different from previous work on Negative Transfer (NT) (Wang et al., 2019; Zhang et al., 2022), we further divide NT in MTL into two types.

Definition 2.2 (Weak Negative Transfer, WNT). For some MTL algorithm \mathcal{A} with weighting hyper-parameter λ , WNT occurs if $TG(\lambda, \mathcal{A}) < 0$.

Definition 2.3 (Strong Negative Transfer, SNT). For some MTL algorithm \mathcal{A} , SNT occurs if $\max_{\lambda > 0} TG(\lambda, \mathcal{A}) < 0$.

Figure 2 illustrates the difference between WNT and SNT. The most essential difference is that we might be able to avoid WNT by selecting a proper weighting hyper-parameter λ , yet we cannot avoid SNT in this way.

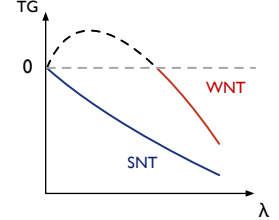


Figure 2. Comparison of WNT and SNT.

Next, we will analyze the negative transfer in MTL from three different perspectives: optimization, generalization, and hypothesis space. In our analysis, we will use task **P** and **Q** in DomainNet (Peng et al., 2019) as target tasks respectively to showcase WNT and SNT, and other tasks in DomainNet as auxiliary tasks. Next, we will present the results of our analysis and please refer to Appendix B for the detailed experiment design.

2.1. Effect of Gradient Conflicts

It is widely believed that gradient conflicts between different tasks will lead to optimization difficulties (Yu et al., 2020a; Liu et al., 2021a), which in turn lead to NT. The degree of gradient conflict is usually measured by the Gradient Cosine Similarity (Yu et al., 2020a; Wang et al., 2021).

Definition 2.4 (Gradient Cosine Similarity, GCS). Denote ϕ_{ij} as the angle between two task gradients \mathbf{g}_i and \mathbf{g}_j , then we define the gradient cosine similarity as $\cos \phi_{ij}$ and the gradients as conflicting when $\cos \phi_{ij} < 0$.

In Figure 1, we plot the correlation curve between GCS and TG. Somewhat counterintuitively, we observe that NT and gradient conflicts are not strongly correlated, and NT might

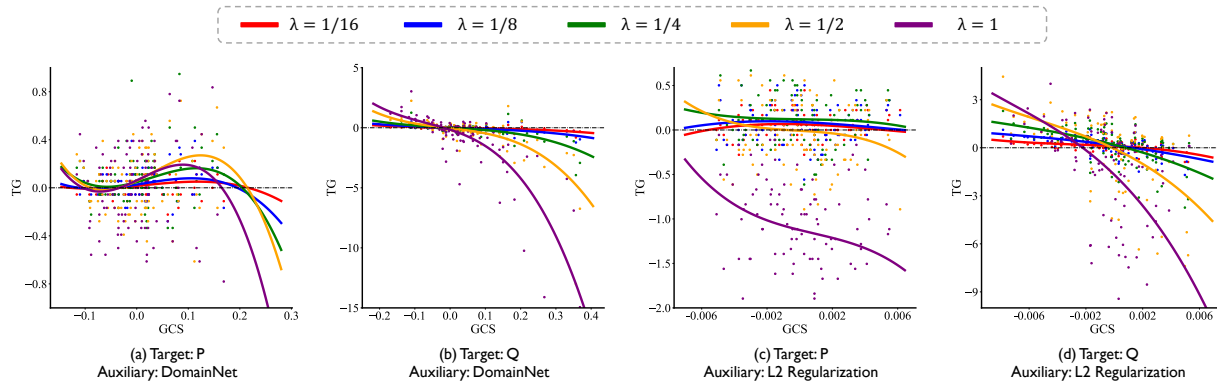


Figure 1. The effect of gradient conflicts. The correlation curve between TG and GCS under different λ . For a fair comparison, each data point starts from the same model parameters in the middle of the training process and updates with one-step multi-task gradient descent.

be severer when the task gradients are highly consistent.

Finding 1. NT is not necessarily caused by gradient conflicts and gradient conflicts do not necessarily lead to NT.

It seems contradictory to the previous work and the reason is that previous work mainly considers the convergence of *optimization* during training, while in our experiments we further consider the *generalization* during evaluation (TG is estimated on the validation set). Although the conflicting gradient of the auxiliary task will increase the training loss of the target task and slow down its convergence speed (Lin et al., 2022), it may also play a role similar to regularization (Kurin et al., 2022), reducing the overfitting of the target task, thereby reducing its generalization error. To confirm our hypothesis, we repeat the above experiments with the auxiliary task replaced by L_2 regularization and observe a similar phenomenon as shown in Figure 1(c)-(d), which indicates that the gradient conflict in MTL is not necessarily harmful, as it may serve as a proper regularization.

Figure 1 also indicates that the weighting hyper-parameter λ in MTL has a large impact on NT. A proper λ not only reduces negative transfer but also promotes positive transfer.

2.2. Effect of Distribution Shift

Next, we will analyze NT from the perspective of generalization. We notice that adjusting λ will change the data distribution that the model is fitting. For instance, when $\lambda = 0$, the model only fits the data distribution of the target task, and when $\lambda = 1$, the model will fit the interpolated distribution of the target and auxiliary tasks. Figure 3(a) quantitatively visualizes the distribution shift under different λ using t-SNE (Van der Maaten & Hinton, 2008). To quantitatively measure the distribution shift in MTL, we

introduce the following definitions.

Following the notations of Mohri & Muñoz Medina (2012), we consider multiclass classification with hypothesis space \mathcal{F} of scoring functions $f : \mathcal{X} \times \mathcal{Y} \rightarrow \mathbb{R}$ where $f(x, y)$ indicates the confidence of predicting x as y .

Definition 2.5 (Confidence Score Discrepancy, CSD). Given scoring function hypothesis \mathcal{F} , denote the optimal hypothesis on distribution P as f_P^* , then CSD between distribution P and Q induced by \mathcal{F} is defined by

$$d_{\mathcal{F}}(P, Q) \triangleq 1 - \mathbb{E}_{x \sim Q} \max_{y \in \mathcal{Y}} f_P^*(x, y). \quad (4)$$

CSD between training and test data indicates how unconfident the model is on the test data, which is expected to increase when the data shift enlarges (Ovadia et al., 2019; Minderer et al., 2021).

Figure 3(b) indicates the correlation between CSD and TG. For WNT tasks, when λ increases at first, the introduced auxiliary tasks will shift the training distribution towards the test distribution, thus decreasing the CSD between training and test data and improving the generalization of the target task. However, when λ continues to increase, the distribution shift gradually increases, finally resulting in NT. For SNT tasks, there is a large gap between the distribution of the introduced auxiliary tasks and that of the target task. Thus, increasing λ always enlarges CSD and always leads to NT. Our above observations are concluded as:

Finding 2. NT is likely to occur if the introduced auxiliary task enlarges the distribution shift between training and test data for the target task.

2.3. Effect of Hypothesis Distance

From the perspective of hypothesis space, models optimized with different λ will converge to different parameters, result-

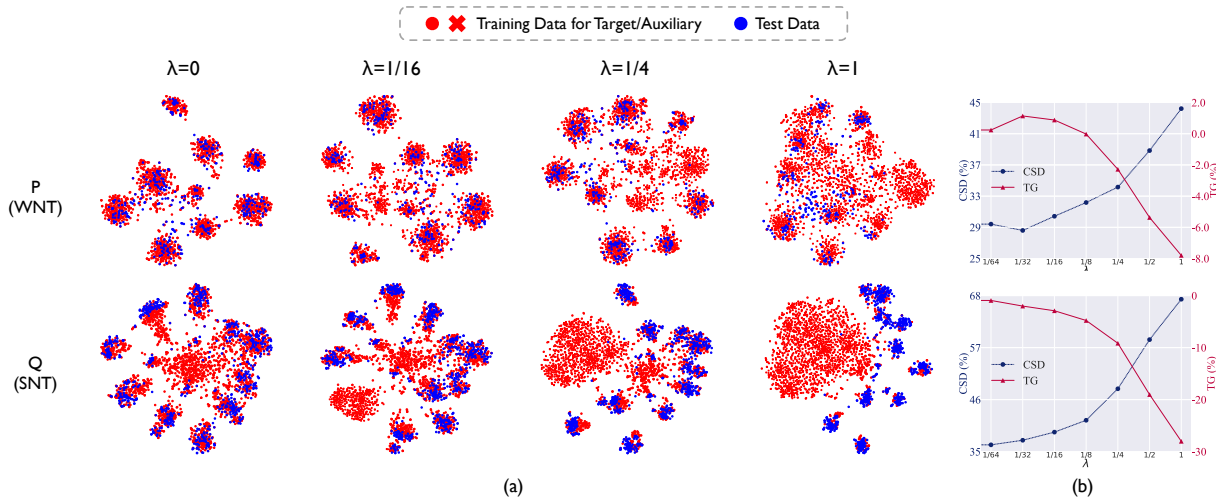


Figure 3. The effect of *distribution shift*. (a) Visualization of **multi-task training distribution** and **target test distribution** under different λ . (b) For WNT tasks, as λ increases, CSD first drops and then rises and TG is first positive and then negative. For SNT tasks, CSD increases monotonically and TG remains negative.

ing in different performances. And we conjecture that the occurrence of NT is related to whether the distance to the optimal hypothesis is reduced. It is hard to verify for deep models, since finding the optimal hypothesis and visualizing the hypothesis space are both difficult. Thus we restrict the original hypothesis space to a simpler hypothesis space.

Definition 2.6 (Linear Combination Hypothesis Space, LCHS). Given a set of M different hypotheses of the same target task $\mathcal{H} = \{h_{\theta_m} | m = 1, \dots, M\}$, the linear combination of the hypotheses in \mathcal{H} forms a new hypothesis space named Linear Combination Hypothesis Space \mathcal{H}_{LC} ,

$$\mathcal{H}_{LC}(\mathcal{H}) = \left\{ h_{\theta} | \theta = \sum_{m=1}^M w_m \theta_m, \sum_{m=1}^M w_m = 1, w_m \geq 0 \right\}. \quad (5)$$

Figure 4 uses the ternary heatmaps to visualize the LCHS of a set of three models including a single-task model and two multi-task models. By enumerating values of \mathbf{w} , we can approximate the optimal hypothesis in LCHS. For WNT tasks, the optimal hypothesis is inside the ternary heatmap, and the closer to the optimal hypothesis, the better the performance will be. Suppose that we are using multi-task learning to optimize the model in the restricted hypothesis space LCHS, a proper λ will reduce the distance to the optimal hypothesis and lead to positive transfer, while an inappropriately large λ enlarging the distance will lead to NT. However, for SNT tasks, the optimal hypothesis in the LCHS is obtained by single-task learning (left-bottom vertex). Therefore, increasing λ will always enlarge the distance to the optimal hypothesis, and NT always exists. In summary:

Finding 3. NT is likely to occur if the introduced auxiliary task enlarges the distance of the learned hypothesis to the optimal hypothesis.

Figure 4 also indicates a good property of deep models: the loss surfaces of over-parameterized deep neural networks are quite well-behaved and smooth after convergence, which has also been mentioned by previous works (Goodfellow et al., 2015; Li et al., 2018) and will be used in our method.

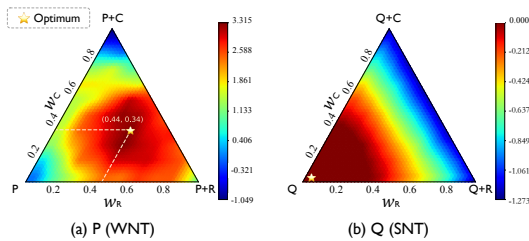


Figure 4. The effect of hypothesis distance. Each triangle vertex represents an optimized model, e.g., P+R is the model jointly optimized with P and R. Each point inside the triangle corresponds to a hypothesis in LCHS and its heat value measures the TG.

3. Methods

Based on our above analysis and findings, we will introduce how to mitigate negative transfer in multi-task learning.

3.1. ForkMerge

First, we consider the case that we have a single target task \mathcal{T}_{tgt} and a single auxiliary task \mathcal{T}_{aux} . When updating the parameters θ_t with Equation (2) at training step t , we have

$$\theta_{t+1}(\lambda) = \theta_t - \eta(\mathbf{g}_{\text{tgt}}(\theta_t) + \lambda \mathbf{g}_{\text{aux}}(\theta_t)), \quad (6)$$

where η is the learning rate, \mathbf{g}_{tgt} and \mathbf{g}_{aux} are the gradients calculated from \mathcal{L}_{tgt} and \mathcal{L}_{aux} respectively. Section 2.1 reveals that the gradient conflict between \mathbf{g}_{tgt} and \mathbf{g}_{aux} does not necessarily lead to NT as long as λ is carefully tuned and Section 2.2 shows that NT is a problem related to generalization. Thus we propose to dynamically adjust λ according to the target validation performance $\hat{\mathcal{P}}$ to avoid NT:

$$\max_{\lambda} \hat{\mathcal{P}}(\theta_{t+1}) = \hat{\mathcal{P}}(\theta_t - \eta(\mathbf{g}_{\text{tgt}}(\theta_t) + \lambda \mathbf{g}_{\text{aux}}(\theta_t))). \quad (7)$$

Equation (7) is a bi-level optimization problem. A typical solution is to first approximate $\hat{\mathcal{P}}$ with the loss of a batch of data on the validation set, and then use first-order approximation to solve λ (Finn et al., 2017; Liu et al., 2022). However, these approximations within a single step of gradient descent introduce large noise to the estimation of λ and also increase the risk of overfitting the validation set.

Inspired by LCHS in Section 2.3, we introduce a new way of approximation. First, we rewrite Equation (7) equally as

$$\max_{\lambda} \hat{\mathcal{P}}((1 - \lambda)\theta_{t+1}(0) + \lambda\theta_{t+1}(1)), \quad (8)$$

where we assume the optimal λ^* satisfies $0 \leq \lambda^* \leq 1$, which can be guaranteed by increasing the scale of \mathcal{L}_{aux} when necessary (see proof of Equation (8) in Appendix A.1). An accurate estimation of performance $\hat{\mathcal{P}}$ in Equation (8)

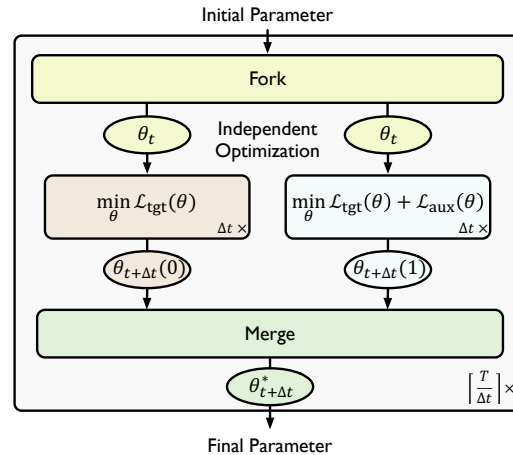


Figure 5. ForkMerge with one target and one auxiliary task.

is still computationally expensive and prone to overfitting, thus we extend the one gradient step to Δt steps,

$$\lambda^* = \max_{\lambda} \widehat{\mathcal{P}}((1 - \lambda)\theta_{t+\Delta t}(0) + \lambda\theta_{t+\Delta t}(1)). \quad (9)$$

Algorithm. As shown in Figure 5, the initial model parameters θ_t at training step t will first be forked into two branches. The first one will be optimized only with the target task loss \mathcal{L}_{tgt} for Δt iterations to obtain $\theta_{t+\Delta t}(0)$, while the other one will be jointly trained for Δt iterations to obtain $\theta_{t+\Delta t}(1)$. Then we will search the optimal λ^* that linearly combines the above two sets of parameters to maximize the validation performance $\widehat{\mathcal{P}}$. Finally, the newly merged parameter $\theta_{t+\Delta t}^* = (1 - \lambda^*)\theta_{t+\Delta t}(0) + \lambda^*\theta_{t+\Delta t}(1)$ will join in a new round, being forked into two branches again and repeating the optimization process for $\lceil \frac{T}{\Delta t} \rceil$ times.

3.2. Scaling ForkMerge to Multiple Tasks

Section 3.1 discusses the case of one target and one auxiliary task and this section will extend to the case of multiple tasks.

Considering that task relationships in MTL are usually asymmetric (see Figure 8), we take each task in turn as the target task and the remaining $K - 1$ tasks as auxiliary tasks to better avoid NT. The objective when optimizing the model for task \mathcal{T}_j is

$$\min_{\theta} \sum_k \lambda_k \mathbb{E}_{\mathcal{T}_k} \mathcal{L}_k(\theta), \quad (10)$$

where $\lambda_j = 1, \sum_{k \neq j} \lambda_k \leq 1$ and $\forall k, \lambda_k \geq 0$. Using gradient descent to update θ_t at training step t , we have

$$\theta_{t+1}(\lambda) = \theta_t - \eta \sum_k \lambda_k \mathbf{g}_k(\theta_t). \quad (11)$$

Given K task-weighting vectors $\{\omega^k\}_{k=1}^K$ that satisfies $\omega_i^k = \mathbb{1}[i = k \text{ or } i = j]$, i.e., the k -th and j -th dimensions of ω^k are 1 and the rest are 0, and a vector Λ that satisfies

$$\Lambda_k = \begin{cases} 1 - \sum_{i \neq j} \lambda_i, & k = j, \\ \lambda_k, & k \neq j, \end{cases} \quad (12)$$

then optimizing λ^* in Equation (11) is equivalent to

$$\Lambda^* = \max_{\Lambda} \widehat{\mathcal{P}}\left(\sum_k \Lambda_k \theta_{t+1}(\omega^k)\right). \quad (13)$$

In Equation (13), the initial model parameters will be forked into K branches, where one branch is optimized with the target task, and the other branches are jointly optimized with one auxiliary task and the target task. Then we will find the optimal Λ^* that linearly combines the K sets of parameters to maximize the validation performance (see proof of Equation (13) and the detailed algorithm in Appendix A.2). Unfortunately, the computational complexity is $\mathcal{O}(K)$, which is unacceptable when K is large.

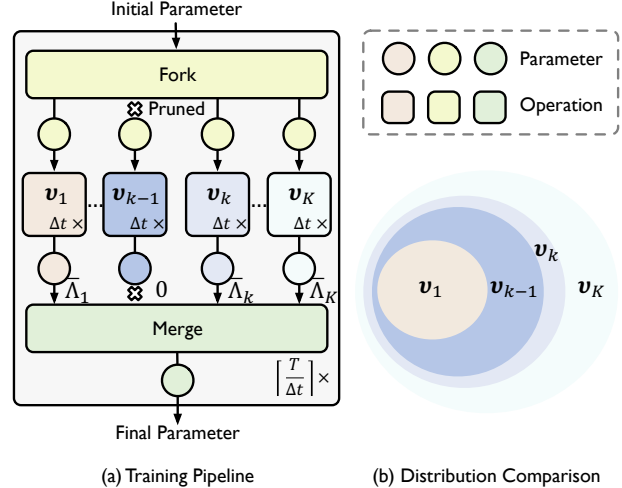


Figure 6. ForkMerge with multiple tasks.

Here we introduce a pruning strategy to reduce the computation cost. First, we sort all the tasks in descending order according to their relevance to the target task \mathcal{T}_j and label them with $1 \sim K$. Obviously, task \mathcal{T}_j will be ranked first. We make the assumption that after sorting, we have $1 = \lambda_1 \geq \lambda_2 \geq \dots \geq \lambda_K \geq 0$ and let $\lambda_{K+1} = 0$. Assume that we have K task-weighting vectors $\{\nu^k\}_{k=1}^K$ that satisfies $\nu_i^k = \mathbb{1}[i \leq k]$, i.e., $\theta_{t+1}(\nu^k)$ will be jointly optimizing with the top k tasks most related to the target task. And define a new vector $\bar{\Lambda}$ that satisfies $\bar{\Lambda}_k = \lambda_k - \lambda_{k+1} \geq 0$, then optimizing λ^* in Equation (11) is equivalent to

$$\bar{\Lambda}^* = \max_{\bar{\Lambda}} \widehat{\mathcal{P}}\left(\sum_k \bar{\Lambda}_k \theta_{t+1}(\nu^k)\right). \quad (14)$$

As mentioned in Section 2.2, the mixture distributions constructed by different ν will result in diverse data shifts from the target distribution, yet we cannot know which ν leads to better generalization in advance. Thus, we convert the problem of mixture distribution into that of mixture hypothesis (Mansour et al., 2008). As shown in Figure 6, we will linearly combine the models trained on different distributions to approach the optimal parameters. By pruning the forking branches with $\bar{\Lambda}_k$ close to 0 and only keeping the branches with the largest $L < K$ values in $\bar{\Lambda}$, we can reduce the time complexity to $\mathcal{O}(L)$. And the definition of ν ensures that most task information is preserved after pruning (see proof of Equation (14) and detailed algorithm in Appendix A.3).

4. Experiments

We evaluate ForkMerge on diverse MTL problems, including molecule graph regression, scene understanding, CTR prediction, and image recognition. Experiment details of this section and additional experimental results are provided in appendixes C and D respectively.

We compare our method with many MTL methods, includ-

Table 1. Performance on QM9 dataset (11 tasks in total).

Methods	μ	α	ϵ_{HOMO}	ϵ_{LUMO}	$\langle R^2 \rangle$	ZPVE	U_0	U	H	G	c_v	$\Delta_m \uparrow$
	MAE \downarrow											
STL	0.066	0.184	60.96	52.58	0.495	4.23	54.7	69.7	58.9	57.3	0.071	-
<i>Methods solving all tasks with a single model</i>												
EW	0.095	0.298	68.36	84.26	4.871	13.23	133.4	134.1	134.5	130.3	0.119	-166.9%
SI	0.309	0.345	149.80	137.50	1.003	4.50	55.3	55.8	55.8	55.3	0.112	-82.1%
UW	0.386	0.425	166.20	155.80	1.060	4.99	66.4	66.8	66.8	66.2	0.122	-112.4%
DWA	0.107	0.325	74.06	90.61	5.090	13.99	142.3	143.0	143.4	139.3	0.125	-183.7%
RLW	0.113	0.340	76.95	92.76	5.860	15.46	156.3	157.1	157.6	153.0	0.137	-213.5%
MGDA	0.202	0.352	121.20	99.57	3.566	5.44	79.1	80.1	79.8	79.3	0.112	-120.6%
GradNorm	0.090	0.286	63.52	80.19	4.804	13.46	128.9	129.7	130.2	125.3	0.115	-160.2%
PCGrad	0.098	0.275	68.71	81.12	3.798	9.11	111.1	111.5	112.0	109.6	0.104	-121.8%
IMTL	0.136	0.287	98.31	93.96	1.750	5.69	101.4	102.4	102.0	100.1	0.096	-82.4%
GradVac	0.083	0.259	64.74	70.42	3.054	7.96	101.5	102.2	102.4	99.8	0.094	-93.2%
CAGrad	0.114	0.323	80.30	96.68	2.973	6.95	108.0	108.8	108.8	106.9	0.116	-110.7%
NashMTL	0.102	0.243	80.93	78.64	2.376	4.92	68.3	68.9	68.8	68.4	0.091	-59.5%
<i>Methods solving each task with a specific model</i>												
GCS	0.091	0.292	65.70	75.45	4.153	12.46	131.3	128.1	129.8	131.1	0.113	-146.8%
Auto- λ	0.067	0.223	58.18	65.30	1.940	7.71	111.4	115.0	118.4	110.9	0.079	-72.0%
PTFT	0.060	0.169	52.12	49.78	0.496	3.04	46.3	47.1	49.3	43.8	0.056	+15.7%
Ours	0.055	0.139	49.96	47.15	0.403	2.78	34.8	35.5	36.1	35.3	0.052	+28.4%

ing: (1) Single Task Learning (STL); (2) Equal Weighting (EW); (3) Loss weighting methods: Scale Invariant (SI) which minimizes logarithm of losses, UW (Kendall et al., 2018), DWA (Liu et al., 2019a), RLW (Lin et al., 2022); (4) Gradient weighting methods: MGDA (Sener & Koltun, 2018), GradNorm (Chen et al., 2018b), PCGrad (Yu et al., 2020a), IMTL (Liu et al., 2021b), GradVac (Wang et al., 2021), CAGrad (Liu et al., 2021a), NashMTL (Navon et al., 2022), GCS (Du et al., 2018), Auto- λ (Liu et al., 2022); (5) PTFT which first Pre-Trains the model by joint training on all the tasks and then Fine-Tunes the model to a specific task. Unless otherwise specified, a specific model is trained for each target task in GCS, Auto- λ , PTFT, and ForkMerge. By default, we use the pruned version of ForkMerge, where $L = \lceil \log_2(K) \rceil$. Each experiment is repeated three times. **We will release the codebase for all the methods.**

Since naturally MTL contains tasks of different types and may have different evaluation metrics for each task, we follow Navon et al. (2022); Lin et al. (2022) and report Δ_m , the average per-task performance improvement of method m (see Definition in Appendix C.1).

4.1. Molecule Graph Regression

We evaluate on a widely used benchmark for molecule property prediction, QM9 (Ramakrishnan et al., 2014), which consists of 11 tasks and $\sim 130\text{K}$ molecules represented as graphs. Following Navon et al. (2022), we use 110K molecules for training, 10K for validation, and 10K for test. Our implementation is based on PyTorch Geometric (Fey & Lenssen, 2019).

Results are shown in Table 1. Most MTL methods lead to severe negative transfer (NT) on this dataset, also observed by previous work (Maron et al., 2019; Johannes Klicpera, 2020; Navon et al., 2022). In contrast, ForkMerge signifi-

Table 2. Performance on NYUv2 dataset (3 tasks in total).

Methods	Segmentation		Depth		Normal	$\Delta_m \uparrow$
	mIoU \uparrow	Pix Acc \uparrow	Abs Err \downarrow	Rel Err \downarrow	Mean \downarrow	
STL	51.42	74.14	41.74	17.37	22.82	-
<i>Methods solving all tasks with a single model</i>						
EW	52.13	74.51	39.03	16.43	24.14	0.30%
UW	52.51	74.72	39.15	16.56	23.99	0.63%
DWA	52.10	74.45	39.26	16.57	24.12	0.07%
RLW	52.88	74.99	39.75	16.67	23.83	0.66%
MGDA	50.79	73.81	39.19	16.25	23.14	1.44%
GradNorm	52.25	74.54	39.31	16.37	23.86	0.56%
PCGrad	51.77	74.72	38.91	16.36	24.31	0.22%
IMTL	52.24	74.73	39.46	15.92	23.25	2.10%
GradVac	52.84	74.77	39.48	16.28	24.00	0.75%
CAGrad	52.04	74.25	39.06	16.30	23.39	1.41%
NashMTL	51.73	74.10	39.55	16.50	23.21	1.11%
<i>Methods solving each task with a specific model</i>						
GCS	52.67	74.59	39.72	16.64	24.10	0.09%
Auto- λ	52.40	74.62	39.25	16.25	23.38	1.17%
PTFT	52.08	74.86	39.58	16.77	22.98	1.49%
Ours	54.30	75.78	38.42	16.11	22.41	4.59%

cantly improves performance on all tasks compared to STL. We also find that PTFT serves as a strong baseline in most of our MTL experiments. Its drawback is that it fails to consider the task relationship in Pre-Training, and suffers from catastrophic forgetting during the Fine-Tuning process.

4.2. Scene Understanding

We evaluate on the widely-used multi-task scene understanding dataset, NYUv2 (Silberman et al., 2012), which contains 3 tasks: 13-class semantic segmentation, depth estimation, and surface normal prediction. Following Navon et al. (2022), we use 636, 159 and 654 images for training, validation, and test. Our implementation is based on LibMTL (Lin & Zhang, 2022) and MTAN (Liu et al., 2019a).

The results are presented in Table 2. NT is not severe on this dataset, where both *segmentation* and *depth* benefit from MTL and only *normal* task gets worse. In such cases, our

Table 3. Performance on AliExpress dataset (2×4 tasks in total).

Architectures	Methods	CTR				CTCVR				Avg	$\Delta_m \uparrow$	
		ES	FR	NL	US	ES	FR	NL	US			
DNN	STL	0.7299	0.7316	0.7237	0.7077	0.8778	0.8682	0.8652	0.8659	0.7963	-	
OMoE	EW	0.7268	0.7211	0.7228	0.7070	0.8878	0.8748	0.8524	0.8796	0.7965	-0.01%	
MMoE		0.7287	0.7244	0.7225	0.7068	0.8874	0.8669	0.8688	0.8742	0.7974	+0.11%	
PLE		0.7309	0.7297	0.7310	0.7090	0.8776	0.8777	0.8741	0.8699	0.8000	+0.45%	
AITM		0.7308	0.7276	0.7264	0.7132	0.7908	0.7746	0.7828	0.7622	0.7510	-5.18%	
<i>Methods solving all tasks with a single model</i>												
DNN	UW	0.7276	0.7235	0.7250	0.7048	0.8814	0.8709	0.8599	0.8793	0.7966	+0.00%	
	DWA	0.7317	0.7284	0.7297	0.7061	0.8663	0.8695	0.8696	0.8484	0.7937	-0.28%	
	RLW	0.7253	0.7225	0.7247	0.7114	0.8874	0.8704	0.8611	0.8455	0.7935	-0.34%	
	MGDA	0.6985	0.6926	0.7000	0.6676	0.8215	0.8145	0.7978	0.7917	0.7480	-5.94%	
	GradNorm	0.7239	0.7178	0.7101	0.7035	0.8851	0.8671	0.8465	0.8685	0.7903	-0.79%	
	PCGrad	0.7209	0.7193	0.7199	0.6892	0.8563	0.8621	0.8479	0.8413	0.7821	-1.76%	
	IMTL	0.7203	0.7193	0.7268	0.6852	0.8472	0.8502	0.8481	0.8282	0.7782	-2.20%	
	GradVac	0.7240	0.7301	0.7227	0.7050	0.8497	0.8623	0.8419	0.7980	0.7792	-1.99%	
	CAGrad	0.7280	0.7271	0.7223	0.6996	0.8712	0.8650	0.8417	0.8648	0.7900	-0.77%	
	NashMTL	0.7229	0.7245	0.7272	0.6972	0.8562	0.8606	0.8667	0.8497	0.7881	-1.00%	
	<i>Methods solving each task with a specific model</i>											
		GCS	0.7229	0.7245	0.7272	0.6972	0.8562	0.8606	0.8667	0.8497	0.7881	-0.49%
		Auto- λ	0.7282	0.7282	0.7263	0.7114	0.8852	0.8646	0.8640	0.8750	0.7979	+0.19%
	PTFT	0.7291	0.7227	0.7244	0.7086	0.8889	0.8808	0.8654	0.8613	0.7977	+0.14%	
	Ours	0.7402	0.7427	0.7416	0.7069	0.8928	0.8786	0.8753	0.8752	0.8067	+1.30%	

method still achieves significant improvement on all tasks.

4.3. CTR and CTCVR Prediction

We evaluate on AliExpress dataset (Li et al., 2020), which consists of 2 tasks: CTR and CTCVR, and 4 scenarios and more than 100M records. Our implementation is based on MTReclib (Zhu et al., 2021). We also compare MTL architectures designed for the click-through rate (CTR), such as OMoE (Jacobs et al., 1991), MMoE (Ma et al., 2018a), PLE (Tang et al., 2020), AITM (Xi et al., 2021).

The results are presented in Table 3. Among all the baselines, increasing the model capacity is one of the most effective strategies. For example, the total number of experts in PLE has increased to 72, with a relative improvement of 0.45%, indicating the difficulty of improvement on such a large-scale dataset. Still, our proposed ForkMerge achieves the best performance with $\Delta_m = 1.30\%$.

4.4. Image Recognition

We also evaluate on the widely-used and also largest multi-domain image recognition dataset, DomainNet (Peng et al., 2019), which contains 6 diverse visual domains and approximately 0.6 million images distributed among 345 categories. In this dataset, the data of different tasks do not overlap. Our implementation is based on TLLib (Jiang et al., 2020).

The results are presented in Table 4. DomainNet contains both positive transfer tasks (C), WNT tasks (I, P, R, S), and SNT tasks (Q). When NT occurs, previous MTL methods lead to severe performance degradation, especially on SNT tasks, while our method can automatically avoid SNT and improve the performance over STL in other cases.

Table 4. Performance on DomainNet dataset (6 tasks in total).

Methods	C	I	P	Q	R	S	Avg	$\Delta_m \uparrow$
STL	77.6	41.4	71.8	73.0	84.6	70.2	69.8	-
<i>Methods solving all tasks with a single model</i>								
EW	78.0	38.1	67.2	50.8	77.1	67.0	63.0	-9.62%
UW	79.1	35.8	68.2	50.5	77.9	67.0	63.1	-9.98%
DWA	78.3	38.2	67.8	51.4	77.3	67.2	63.4	-9.15%
RLW	76.5	36.0	66.5	47.7	77.0	65.1	61.5	-12.1%
MGDA	78.1	37.2	69.2	51.0	80.0	67.3	63.8	-8.80%
GradNorm	78.4	38.9	69.4	52.9	79.0	67.7	64.4	-7.68%
PCGrad	78.3	38.0	68.2	50.4	77.4	67.3	63.3	-9.32%
IMTL	79.4	38.6	68.6	53.7	79.3	67.6	64.5	-7.55%
GradVac	78.1	38.3	67.7	51.1	77.0	67.3	63.3	-9.28%
CAGrad	79.1	38.6	69.4	53.6	79.8	67.6	64.7	-7.35%
NashMTL	71.8	32.9	62.2	39.5	73.5	61.4	56.9	-18.8%
<i>Methods solving each task with a specific model</i>								
GCS	74.6	36.0	67.6	56.6	76.4	62.3	62.3	-11.0%
Auto- λ	78.3	37.8	70.2	56.3	79.7	67.1	64.9	-7.18%
PTFT	78.7	42.3	72.7	73.0	84.7	71.2	70.4	+1.07%
Ours	81.1	44.0	73.7	73.0	85.2	72.7	71.6	+3.00%

4.5. Analysis

To further investigate how ForkMerge improves MTL performance, we conduct further analysis on NYUv2.

The merging step Δt that is too large or too small is not optimal. As shown in Figure 7, ForkMerge is optimal when $\Delta t = 10$ epochs. When Δt is small, the estimation of λ is short-sighted and might fail to remove the harmful parameter updates when NT occurs, which also indicates the limitations of methods that use single-step gradient descent to estimate λ . When Δt is large, the risk to get bad model parameters from the linear combination will also increase.

Task relationships are asymmetric. Following Standley et al. (2020), we visualize the pairwise relationships measured by TG with different MTL algorithms in Figure 8. We have two conclusions: (1) The task relationships in MTL are asymmetric, thus it is better to distinguish the target from

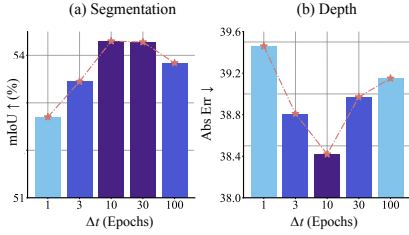


Figure 7. The effect of merging epochs Δt .

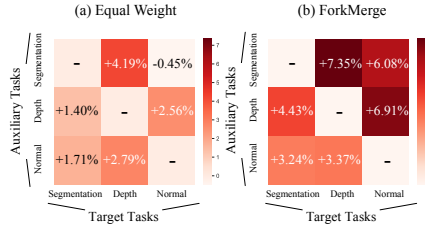


Figure 8. Task relationships.

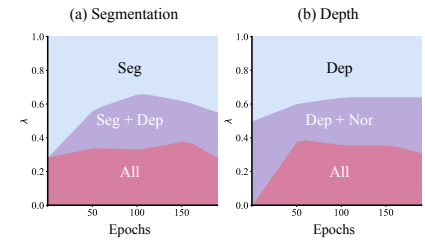


Figure 9. Importance of each forking branch.

the auxiliary to avoid NT. (2) Our method also works well with a single auxiliary task.

The importance of different forking branches is dynamic. As shown in Figure 9, the relative ratio of each forking branch is dynamic and varies from task to task, which indicates the importance of the dynamic merge mechanism.

5. Related Work

5.1. Multi-Task Learning

Multi-Task Architectures. To effectively boost information sharing and alleviate task conflict, significant efforts have been invested in multi-task architecture design. Existing techniques can be categorized into hard-parameter sharing (Kokkinos, 2017; He et al., 2017; Heuer et al., 2021) and soft-parameter sharing (Misra et al., 2016; Rusu et al., 2016; Fernando et al., 2017; Ma et al., 2018a; Liu et al., 2019a; Maninis et al., 2019; Tang et al., 2020). And our work is agnostic and complementary to these designs.

Multi-Task Optimization Strategies. An orthogonal generation of work aims to improve optimization strategies. *Loss balancing* and *gradient balancing* methods propose to find suitable task weighting through various criteria, such as task uncertainty (Kendall et al., 2018), task loss magnitudes (Liu et al., 2019a), gradient norm (Chen et al., 2018b), and gradient directions (Yu et al., 2020a; Chen et al., 2020; Liu et al., 2021a;b; Javaloy & Valera, 2022; Navon et al., 2022). The above criteria mainly alleviate the optimization difficulty while the validation performance criterion in our method further considers the generalization problem in MTL.

To find the proper tasks for multi-task learning, recent work explores task relationships by *task grouping* (Zamir et al., 2018; Standley et al., 2020; Fifty et al., 2021; Song et al., 2022), where positively related tasks are trained together and unrelated tasks are assigned to different groups to avoid interference with each other. The task relationships in these methods are fixed during training and limited to only binary possibilities (trainer together or trained separately). In contrast, the task relationships in our method are *dynamic* in time and closer to *continuous* in values (see Figure 9),

which are more flexible and effective (see Figure 8).

The most related works to ours are GCS (Du et al., 2018) and Auto- λ (Liu et al., 2022), which estimate one-step task weighting through gradient cosine similarity and finite-difference approximation (Finn et al., 2017), respectively. The main differences between our method and theirs are two folds: (1) The task weighting in GCS and Auto- λ is determined by the interactions between task gradients from the optimization perspective. Whereas in our method, the task weighting is determined by the performance gain brought by different tasks from the generalization perspective. (2) Auto- λ or GCS focus on *short-term* gains of MTL, while our method considers the *long-term* benefits, which greatly impacts the final performance (see Figure 7).

5.2. Negative Transfer

Negative Transfer (NT) is a widely existing phenomenon in machine learning, where transferring knowledge from the source data or model can have negative impact on the target learner (Rosenstein, 2005; Pan & Yang, 2010; Jiang et al., 2022). To mitigate NT, domain adaptation methods (Wang et al., 2019; Zhang et al., 2018) design importance sampling or instance weighting strategies to prioritize related source data. Fine-tuning methods (Chen et al., 2019) filter out detrimental pre-trained knowledge by suppressing untransferable spectral components in the representation. MTL methods use gradient surgery (Yu et al., 2020a; Wang et al., 2021; Javaloy & Valera, 2022) or task weighting (Liu et al., 2019b) to reduce the gradient conflicts across tasks. Different from previous work, we propose to dynamically filter out harmful parameter updates in the training process to avoid NT. Besides, we provide an in-depth experimental analysis of the causes of NT in MTL, which is rare in this field yet will be helpful for future research.

6. Conclusion

Many methods have been proposed to mitigate negative transfer in multi-task learning, yet there is still a lack of in-depth experimental analysis on the causes of negative transfer. In this paper, we systematically delved into the negative transfer issues and present ForkMerge, a novel approach to avoid negative transfer in multi-task learning.

Experimentally, ForkMerge achieves state-of-the-art performance on four different multi-task learning benchmarks.

References

- Baxter, J. A model of inductive bias learning. *Journal of artificial intelligence research*, 2000.
- Caruana, R. Multitask learning. *Machine Learning*, 28: 41–75, 1997.
- Chen, L., Zhu, Y., Papandreou, G., Schroff, F., and Adam, H. Encoder-decoder with atrous separable convolution for semantic image segmentation. In *ECCV*, 2018a.
- Chen, X., Wang, S., Fu, B., Long, M., and Wang, J. Catastrophic forgetting meets negative transfer: Batch spectral shrinkage for safe transfer learning. In *NeurIPS*, 2019.
- Chen, Z., Badrinarayanan, V., Lee, C.-Y., and Rabinovich, A. Gradnorm: Gradient normalization for adaptive loss balancing in deep multitask networks. In *ICML*, 2018b.
- Chen, Z., Ngiam, J., Huang, Y., Luong, T., Kretzschmar, H., Chai, Y., and Anguelov, D. Just pick a sign: Optimizing deep multitask models with gradient sign dropout. In *NeurIPS*, 2020.
- Deng, J., Dong, W., Socher, R., Li, L.-J., Li, K., and Fei-Fei, L. Imagenet: A large-scale hierarchical image database. In *CVPR*, 2009.
- Du, Y., Czarnecki, W. M., Jayakumar, S. M., Farajtabar, M., Pascanu, R., and Lakshminarayanan, B. Adapting auxiliary losses using gradient similarity. *arXiv preprint arXiv:1812.02224*, 2018.
- Fernando, C., Banarse, D., Blundell, C., Zwols, Y., Ha, D., Rusu, A. A., Pritzel, A., and Wierstra, D. Pathnet: Evolution channels gradient descent in super neural networks. *CoRR*, abs/1701.08734, 2017.
- Fey, M. and Lenssen, J. E. Fast graph representation learning with PyTorch Geometric. In *ICLR Workshop on Representation Learning on Graphs and Manifolds*, 2019.
- Fifty, C., Amid, E., Zhao, Z., Yu, T., Anil, R., and Finn, C. Efficiently identifying task groupings for multi-task learning. In *NeurIPS*, 2021.
- Finn, C., Abbeel, P., and Levine, S. Model-agnostic meta-learning for fast adaptation of deep networks. In *ICML*, 2017.
- Gilmer, J., Schoenholz, S. S., Riley, P. F., Vinyals, O., and Dahl, G. E. Neural message passing for quantum chemistry. In *ICML*, 2017.
- Goodfellow, I., Vinyals, O., and Saxe, A. Qualitatively characterizing neural network optimization problems. In *ICLR*, 2015.
- Goyal, P., Dollár, P., Girshick, R. B., Noordhuis, P., Wesolowski, L., Kyrola, A., Tulloch, A., Jia, Y., and He, K. Accurate, large minibatch SGD: training imagenet in 1 hour. *arXiv preprint arXiv:1706.02677*, 2017.
- He, K., Zhang, X., Ren, S., and Sun, J. Deep residual learning for image recognition. In *CVPR*, 2016.
- He, K., Gkioxari, G., Dollár, P., and Girshick, R. Mask r-cnn. In *ICCV*, 2017.
- Heuer, F., Mantowsky, S., Bukhari, S., and Schneider, G. Multitask-centernet (mcn): Efficient and diverse multi-task learning using an anchor free approach. In *ICCV*, 2021.
- Jacobs, R. A., Jordan, M. I., Nowlan, S. J., and Hinton, G. E. Adaptive mixtures of local experts. *Neural computation*, 1991.
- Javaloy, A. and Valera, I. Rotograd: Gradient homogenization in multitask learning. In *ICLR*, 2022.
- Jiang, J., Chen, B., Fu, B., and Long, M. Transfer-learning-library. <https://github.com/thuml/Transfer-Learning-Library>, 2020.
- Jiang, J., Shu, Y., Wang, J., and Long, M. Transferability in deep learning: A survey. *arXiv preprint arXiv:2201.05867*, 2022.
- Johannes Klicpera, Janek Groß, S. G. Directional message passing for molecular graphs. In *ICLR*, 2020.
- Kendall, A., Gal, Y., and Cipolla, R. Multi-task learning using uncertainty to weigh losses for scene geometry and semantics. In *CVPR*, 2018.
- Kingma, D. P. and Ba, J. Adam: A method for stochastic optimization. In *ICLR*, 2015.
- Kokkinos, I. Ubertnet: Training a ‘universal’ convolutional neural network for low-, mid-, and high-level vision using diverse datasets and limited memory. In *CVPR*, 2017.
- Kurin, V., De Palma, A., Kostrikov, I., Whiteson, S., and Kumar, M. P. In defense of the unitary scalarization for deep multi-task learning. In *NeurIPS*, 2022.
- Li, H., Xu, Z., Taylor, G., Studer, C., and Goldstein, T. Visualizing the loss landscape of neural nets. In *NeurIPS*, 2018.
- Li, P., Li, R., Da, Q., Zeng, A.-X., and Zhang, L. Improving multi-scenario learning to rank in e-commerce by exploiting task relationships in the label space. In *CIKM*, 2020.

- Lin, B. and Zhang, Y. LibMTL: A python library for multi-task learning. *arXiv preprint arXiv:2203.14338*, 2022.
- Lin, B., Feiyang, Y., Zhang, Y., and Tsang, I. Reasonable effectiveness of random weighting: A litmus test for multi-task learning. In *TMLR*, 2022.
- Liu, B., Liu, X., Jin, X., Stone, P., and Liu, Q. Conflict-averse gradient descent for multi-task learning. In *NeurIPS*, 2021a.
- Liu, L., Li, Y., Kuang, Z., Xue, J., Chen, Y., Yang, W., Liao, Q., and Zhang, W. Towards impartial multi-task learning. In *ICLR*, 2021b.
- Liu, S., Johns, E., and Davison, A. J. End-to-end multi-task learning with attention. In *CVPR*, 2019a.
- Liu, S., Liang, Y., and Gitter, A. Loss-balanced task weighting to reduce negative transfer in multi-task learning. In *AAAI*, 2019b.
- Liu, S., James, S., Davison, A. J., and Johns, E. Auto-lambda: Disentangling dynamic task relationships. In *TMLR*, 2022.
- Liu, X., He, P., Chen, W., and Gao, J. Multi-task deep neural networks for natural language understanding. In *ACL*, 2019c.
- Loshchilov, I. and Hutter, F. SGDR: stochastic gradient descent with warm restarts. In *ICLR*, 2017.
- Ma, J., Zhao, Z., Yi, X., Chen, J., Hong, L., and Chi, E. H. Modeling task relationships in multi-task learning with multi-gate mixture-of-experts. In *SIGKDD*, 2018a.
- Ma, X., Zhao, L., Huang, G., Wang, Z., Hu, Z., Zhu, X., and Gai, K. Entire space multi-task model: An effective approach for estimating post-click conversion rate. In *SIGIR*, 2018b.
- Maninis, K.-K., Radosavovic, I., and Kokkinos, I. Attentive single-tasking of multiple tasks. In *CVPR*, 2019.
- Mansour, Y., Mohri, M., and Rostamizadeh, A. Domain adaptation with multiple sources. In *NIPS*, 2008.
- Maron, H., Ben-Hamu, H., Serviansky, H., and Lipman, Y. Provably powerful graph networks. In *NeurIPS*, 2019.
- Minderer, M., Djolonga, J., Romijnders, R., Hubis, F., Zhai, X., Houlsby, N., Tran, D., and Lucic, M. Revisiting the calibration of modern neural networks. In *NeurIPS*, 2021.
- Misra, I., Shrivastava, A., Gupta, A., and Hebert, M. Cross-stitch networks for multi-task learning. In *CVPR*, 2016.
- Mohri, M. and Muñoz Medina, A. New analysis and algorithm for learning with drifting distributions. In *International Conference on Algorithmic Learning Theory*, 2012.
- Navon, A., Shamsian, A., Achituve, I., Maron, H., Kawaguchi, K., Chechik, G., and Fetaya, E. Multi-task learning as a bargaining game. In *ICML*, 2022.
- Ovadia, Y., Fertig, E., Ren, J., Nado, Z., Sculley, D., Nowozin, S., Dillon, J., Lakshminarayanan, B., and Snoek, J. Can you trust your model’s uncertainty? evaluating predictive uncertainty under dataset shift. In *NeurIPS*, 2019.
- Pan, S. J. and Yang, Q. A survey on transfer learning. In *TKDE*, 2010.
- Peng, X., Bai, Q., Xia, X., Huang, Z., Saenko, K., and Wang, B. Moment matching for multi-source domain adaptation. *ICCV*, 2019.
- Ramakrishnan, R., Dral, P. O., Rupp, M., and Von Lilienfeld, O. A. Quantum chemistry structures and properties of 134 kilo molecules. *Scientific data*, 2014.
- Rosenstein, M. T. To transfer or not to transfer. In *NeurIPS*, 2005.
- Rusu, A. A., Rabinowitz, N. C., Desjardins, G., Soyer, H., Kirkpatrick, J., Kavukcuoglu, K., Pascanu, R., and Hadsell, R. Progressive neural networks. *CoRR*, abs/1606.04671, 2016.
- Sener, O. and Koltun, V. Multi-task learning as multi-objective optimization. In *NeurIPS*, 2018.
- Silberman, N., Hoiem, D., Kohli, P., and Fergus, R. Indoor segmentation and support inference from rgb-d images. In *ECCV*, 2012.
- Song, X., Zheng, S., Cao, W., Yu, J., and Bian, J. Efficient and effective multi-task grouping via meta learning on task combinations. In *NeurIPS*, 2022.
- Standley, T., Zamir, A., Chen, D., Guibas, L. J., Malik, J., and Savarese, S. Which tasks should be learned together in multi-task learning? In *ICML*, 2020.
- Tang, H., Liu, J., Zhao, M., and Gong, X. Progressive layered extraction (ple): A novel multi-task learning (mtl) model for personalized recommendations. In *RecSys*, 2020.
- Van der Maaten, L. and Hinton, G. Visualizing data using t-sne. In *JMLR*, 2008.
- Wang, Z., Dai, Z., Póczos, B., and Carbonell, J. Characterizing and avoiding negative transfer. In *CVPR*, 2019.

- Wang, Z., Tsvetkov, Y., Firat, O., and Cao, Y. Gradient vaccine: Investigating and improving multi-task optimization in massively multilingual models. In *ICLR*, 2021.
- Xi, D., Chen, Z., Yan, P., Zhang, Y., Zhu, Y., Zhuang, F., and Chen, Y. Modeling the sequential dependence among audience multi-step conversions with multi-task learning in targeted display advertising. In *SIGKDD*, 2021.
- Xin, D., Ghorbani, B., Gilmer, J., Garg, A., and Firat, O. Do current multi-task optimization methods in deep learning even help? In *NeurIPS*, 2022.
- You, Y., Li, J., Hseu, J., Song, X., Demmel, J., and Hsieh, C. Reducing BERT pre-training time from 3 days to 76 minutes. In *ICLR*, 2020.
- Yu, T., Kumar, S., Gupta, A., Levine, S., Hausman, K., and Finn, C. Gradient surgery for multi-task learning. In *NeurIPS*, 2020a.
- Yu, T., Quillen, D., He, Z., Julian, R., Hausman, K., Finn, C., and Levine, S. Meta-world: A benchmark and evaluation for multi-task and meta reinforcement learning. In *CORL*, 2020b.
- Zamir, A. R., Sax, A., Shen, W. B., Guibas, L. J., Malik, J., and Savarese, S. Taskonomy: Disentangling task transfer learning. In *CVPR*, 2018.
- Zhang, J., Ding, Z., Li, W., and Ogunbona, P. Importance weighted adversarial nets for partial domain adaptation. In *CVPR*, 2018.
- Zhang, W., Deng, L., Zhang, L., and Wu, D. A survey on negative transfer. *IEEE/CAA Journal of Automatica Sinica*, 2022.
- Zhu, Y., Liu, Y., Xie, R., Zhuang, F., Hao, X., Ge, K., Zhang, X., Lin, L., and Cao, J. Learning to expand audience via meta hybrid experts and critics for recommendation and advertising. In *KDD*, 2021.

A. Algorithm Details

A.1. ForkMerge with a single target and a single auxiliary task

Proof of Equation (8).

$$\begin{aligned}
 \lambda^* &= \max_{\lambda} \widehat{\mathcal{P}}(\theta_{t+1}) \\
 &= \max_{\lambda} \widehat{\mathcal{P}}(\theta_t - \eta(\mathbf{g}_{\text{tgt}}(\theta_t) + \lambda \mathbf{g}_{\text{aux}}(\theta_t))) \\
 &= \max_{\lambda} \widehat{\mathcal{P}}((\theta_t - \eta \mathbf{g}_{\text{tgt}}(\theta_t)) + \lambda(-\eta \mathbf{g}_{\text{aux}}(\theta_t))) \\
 &= \max_{\lambda} \widehat{\mathcal{P}}((1 - \lambda)(\theta_t - \eta \mathbf{g}_{\text{tgt}}(\theta_t)) + \lambda(\theta_t - \eta(\mathbf{g}_{\text{tgt}}(\theta_t) + \mathbf{g}_{\text{aux}}(\theta_t)))) \\
 &= \max_{\lambda} \widehat{\mathcal{P}}((1 - \lambda)\theta_{t+1}(0) + \lambda\theta_{t+1}(1)),
 \end{aligned}$$

Detailed Algorithm.

Algorithm 1 Fork_Merge_v0

Input: initial model parameter θ_0 , total iterations T , interval Δt , auxiliary task index aux , target task index tgt

Output: final model parameter θ_T^* , task relevance λ^*

```

1: fork model into 2 copies  $\{\theta^l\}_{l=0}^1$ 
2: for  $l = 0$  to 1 do
3:    $\theta_0^l \leftarrow \theta_0$  ▷ initialization
4: end for
5: while  $t < T$  do
6:   for  $l = 0$  to 1 do ▷ independent update
7:     for  $t' = t$  to  $t + \Delta t - 1$  do
8:        $\theta_{t'+1}^l = \theta_{t'}^l - \eta(\mathbf{g}_{\text{tgt}}(\theta_{t'}^l) + l \cdot \mathbf{g}_{\text{aux}}(\theta_{t'}^l))$ 
9:     end for
10:   end for
11:    $\lambda^* \leftarrow \max_{\lambda} \widehat{\mathcal{P}}((1 - \lambda)\theta_{t+\Delta t}^0 + \lambda\theta_{t+\Delta t}^1)$  ▷ search  $\lambda$  on the validation set
12:
13:    $\theta_{t+\Delta t}^* \leftarrow (1 - \lambda^*)\theta_{t+\Delta t}^0 + \lambda^*\theta_{t+\Delta t}^1$  ▷ merge parameters
14:
15:   for  $l = 0$  to 1 do ▷ synchronize parameters
16:      $\theta_{t+\Delta t}^l \leftarrow \theta_{t+\Delta t}^*$ 
17:   end for
18:    $t \leftarrow t + \Delta t$ 
19: end while
    
```

Remarks on the search step.

We provide two search strategies as follows, which work well in our experiments.

- *Grid Search:* Exhaustively searching the task-weighting hyper-parameter λ through a manually specified subset of the hyperparameter space, such as $\{0, 0.2, 0.4, 0.6, 0.8, 1.0\}$.
- *Binary Search:* Repeatedly dividing the search interval of λ in half and keep the better hyperparameter.

Random search, bayesian optimization, gradient-based optimization, and other hyper-parameter optimization methods can also be used here, and they are left to be explored in follow-up work.

In practice, the costs of estimating $\widehat{\mathcal{P}}$ in the search step are usually negligible. Yet when the amount of data in the validation set is relatively large, we can sample the validation set to reduce the cost of estimating $\widehat{\mathcal{P}}$.

Remarks on extension from the one gradient step to Δt steps.

1. It can effectively reduce the average cost of estimating $\widehat{\mathcal{P}}$ at each step and avoid overfitting the validation set.
2. It allows longer-term rewards from auxiliary tasks and leads to safer task transfer. For instance, when the accumulated gradients of some auxiliary tasks are harmful to the final target performance, the merging step can cancel the effect of these auxiliary tasks by setting their associated weights λ to 0, to avoid SNT.
3. It increases the risk to produce bad model parameters. However, such risk is still low since deep models usually have smooth loss surfaces after convergence as mentioned in Section 2.3.

In the implementation, we make the following designs to reduce the risk to produce bad model parameters: (1) The models in all forks will start from the same initialization; (2) The models in all forks will be optimized toward the target task. (3) We will use the validation set to pick a proper Δt for each dataset and use it for all tasks in this dataset.

Figure 7 also illustrates that an appropriate Δt can effectively promote the performance of the ForkMerge algorithm, indicating the necessity of the extension from the one gradient step in previous work to Δt steps.

A.2. ForkMerge with a single target and multiple auxiliary tasks
Proof of Equation (13).

The goal of selecting λ^* in Equation (11) is to maximize the validation performance of model θ_{t+1} ,

$$\begin{aligned}
 \lambda^* &= \max_{\lambda} \widehat{\mathcal{P}}(\theta_{t+1}) \\
 &= \max_{\lambda} \widehat{\mathcal{P}}(\theta_t - \eta \sum_k \lambda_k \mathbf{g}_k(\theta_t)) && // \text{gradient descent} \\
 &= \max_{\lambda} \widehat{\mathcal{P}}(\theta_t - \eta \lambda_j \mathbf{g}_j(\theta_t) - \eta \sum_{k \neq j} \lambda_k \mathbf{g}_k(\theta_t)) \\
 &= \max_{\lambda} \widehat{\mathcal{P}}(\theta_t - \eta \mathbf{g}_j(\theta_t) - \eta \sum_{k \neq j} \lambda_k \mathbf{g}_k(\theta_t)) && // \lambda_j = 1 \\
 &= \max_{\lambda} \widehat{\mathcal{P}}((1 - \sum_{k \neq j} \lambda_k)(\theta_t - \eta \mathbf{g}_j(\theta_t)) + (\sum_{k \neq j} \lambda_k)(\theta_t - \eta \mathbf{g}_j(\theta_t)) + \sum_{k \neq j} \lambda_k (-\eta \mathbf{g}_k(\theta_t))) && // \sum_{k \neq j} \lambda_k \leq 1 \\
 &= \max_{\lambda} \widehat{\mathcal{P}}((1 - \sum_{k \neq j} \lambda_k)(\theta_t - \eta \mathbf{g}_j(\theta_t)) + \sum_{k \neq j} \lambda_k (\theta_t - \eta \mathbf{g}_j(\theta_t) - \eta \mathbf{g}_k(\theta_t)))
 \end{aligned}$$

By definitions of Λ and $\{\omega^k\}_{k=1}^K$

$$\Lambda_k = \begin{cases} 1 - \sum_{i \neq j} \lambda_i, & k = j, \\ \lambda_k, & k \neq j, \end{cases}$$

$$\omega_i^k = \begin{cases} 1, & i = j \text{ or } i = k, \\ 0, & \text{otherwise,} \end{cases}$$

we can prove that optimizing λ in Equation (11) is equivalent to optimizing Λ as follows:

$$\Lambda^* = \max_{\Lambda} \widehat{\mathcal{P}}\left(\sum_k \Lambda_k \theta_{t+1}(\omega^k)\right).$$

Detailed Algorithm. Algorithms 2 provides the general optimization process for any task-weighting vector $\{\omega^l\}_{l=1}^L$. When pruning strategy is not used, we have $\omega_i^k = \mathbb{1}[i = k \text{ or } i = j]$.

Algorithm 2 Fork_Merge_v1

Input: initial model parameter θ_0 , task-weighting vector $\{\omega^l\}_{l=1}^L$, total iterations T , interval Δt , number of tasks K , target task index j

Output: final model parameter θ_T^* , task relationship Λ^*

- 1: fork model into L copies $\{\theta^l\}_{l=1}^L$
- 2: **for** $l = 1$ **to** L **do**
- 3: $\theta_0^l \leftarrow \theta_0$ ▷ initialization
- 4: **end for**
- 5: **while** $t < T$ **do**
- 6: **for** $l = 1$ **to** L **do** ▷ independent update
- 7: **for** $t' = t$ **to** $t + \Delta t - 1$ **do**
- 8: $\theta_{t'+1}^l = \theta_{t'}^l - \eta \sum_k \omega_k^l \mathbf{g}_k(\theta_{t'}^l)$
- 9: **end for**
- 10: **end for**
- 11: $\Lambda^* \leftarrow \max_{\Lambda} \widehat{\mathcal{P}}(\sum_l \Lambda_l \theta_{t+\Delta t}^l)$
- 12: ▷ search Λ on the validation set
- 13: $\theta_{t+\Delta t}^* \leftarrow \sum_l \Lambda_l^* \theta_{t+\Delta t}^l$
- 14: ▷ merge parameters
- 15: **for** $l = 1$ **to** L **do**
- 16: $\theta_{t+\Delta t}^l \leftarrow \theta_{t+\Delta t}^*$ ▷ synchronize parameters
- 17: **end for**
- 18: $t \leftarrow t + \Delta t$
- 19: **end while**

Remarks on the search steps.

Grid searching all possible values of Λ is computationally expensive especially when $\|\Lambda\|$ is large. Thus, here we introduce a greedy search strategy in Algorithm 3, which reduces the computation complexity from exponential complexity to $\mathcal{O}(\|\Lambda\|)$.

Algorithm 3 Greedy Search of Λ^*

Input: A list of model parameters $\theta_1, \dots, \theta_L$ sorted in decreasing order of $\widehat{\mathcal{P}}(\theta_l)$.

Output: optimal linear combination coefficient Λ^*

- 1: unnormalized combination coefficient $\tilde{\Lambda} \leftarrow \mathbf{e}_1$ ▷ initialization
- 2: **for** $l = 2$ **to** L **do**
- 3: set upper bound $U \leftarrow \frac{1}{l-1} \sum_{m=1}^{l-1} \tilde{\Lambda}_m$
- 4: grid search the optimal $\tilde{\Lambda}_m$ in range $[0, U]$ to maximize $\widehat{\mathcal{P}}(\frac{1}{\|\tilde{\Lambda}\|} \sum_{m=1}^l \tilde{\Lambda}_m \theta_m)$
- 5: **end for**
- 6: $\Lambda^* \leftarrow \frac{1}{\|\tilde{\Lambda}\|} \tilde{\Lambda}$ ▷ normalization

A.3. Pruned ForkMerge with a single target and multiple auxiliary tasks

Proof of Equation (14).

The goal of selecting λ^* in Equation (11) is to maximize the validation performance of model θ_{t+1} ,

$$\begin{aligned}
 \lambda^* &= \max_{\lambda} \widehat{\mathcal{P}}(\theta_{t+1}) \\
 &= \max_{\lambda} \widehat{\mathcal{P}}\left(\theta_t - \eta \sum_{k=1}^K \lambda_k \mathbf{g}_k(\theta_t)\right) && // \text{gradient descent} \\
 &= \max_{\lambda} \widehat{\mathcal{P}}\left((\lambda_1 - \lambda_{K+1})\theta_t - \eta \sum_{k=1}^K (\lambda_k - \lambda_{K+1}) \mathbf{g}_k(\theta_t)\right) && // \lambda_1 = 1, \lambda_{K+1} = 0 \\
 &= \max_{\lambda} \widehat{\mathcal{P}}\left(\left(\sum_{k=1}^K (\lambda_k - \lambda_{k+1})\right)\theta_t - \eta \sum_{k=1}^K \left(\sum_{i=k}^K (\lambda_i - \lambda_{i+1})\right) \mathbf{g}_k(\theta_t)\right) \\
 &= \max_{\lambda} \widehat{\mathcal{P}}\left(\left(\sum_{k=1}^K (\lambda_k - \lambda_{k+1})\right)\theta_t - \eta \sum_{i=1}^K \sum_{k=1}^i ((\lambda_i - \lambda_{i+1}) \mathbf{g}_k(\theta_t))\right) && // \text{swap summation order} \\
 &= \max_{\lambda} \widehat{\mathcal{P}}\left(\left(\sum_{k=1}^K (\lambda_k - \lambda_{k+1})\right)\theta_t - \eta \sum_{k=1}^K \sum_{i=1}^k ((\lambda_k - \lambda_{k+1}) \mathbf{g}_i(\theta_t))\right) && // \text{swap } k \text{ and } i \\
 &= \max_{\lambda} \widehat{\mathcal{P}}\left(\sum_{k=1}^K (\lambda_k - \lambda_{k+1})\theta_t - \eta \sum_{k=1}^K (\lambda_k - \lambda_{k+1}) \left(\sum_{i=1}^k \mathbf{g}_i(\theta_t)\right)\right) \\
 &= \max_{\lambda} \widehat{\mathcal{P}}\left(\sum_{k=1}^K (\lambda_k - \lambda_{k+1}) \left(\theta_t - \eta \left(\sum_{i=1}^k \mathbf{g}_i(\theta_t)\right)\right)\right)
 \end{aligned}$$

By definitions of Λ and $\{\nu^k\}_{k=1}^K$

$$\bar{\Lambda}_k = \lambda_k - \lambda_{k+1} \quad (15)$$

$$\nu_i^k = \mathbb{1}[i \leq k] \quad (16)$$

we can prove that optimizing λ in Equation (11) is equivalent to optimizing $\bar{\Lambda}$ as follows:

$$\bar{\Lambda}^* = \max_{\bar{\Lambda}} \widehat{\mathcal{P}}\left(\sum_k \bar{\Lambda}_k \theta_{t+1}(\nu^k)\right). \quad (17)$$

Detailed Algorithm.

Algorithm 4 implements the pruned version of ForkMerge based on Algorithms 1 and 2.

In practice, we choose $L = \lceil \log_2(K) \rceil$ and always keep branches with weighting vector ν_K (jointly trained on all tasks) to ensure that the information of all tasks is preserved after pruning. We also keep branch ν_1 (trained only with target task), such that when the NT happens, the parameters of the model can be restored through the merge step, which can effectively avoid NT.

A.4. ForkMerge with multiple target and auxiliary tasks

To find the optimal θ that have an overall good performance across all tasks $\{\mathcal{T}_j\}_{j=1}^K$, we first construct a pseudo target task \mathcal{T}_0 , with loss function $\mathcal{L}_0 = \frac{1}{K} \sum_{j=1}^K \mathcal{L}_j$ and performance measure $\widehat{\mathcal{P}}_0 = \sum_{j=1}^K \widehat{\mathcal{P}}_j$, and then directly use Algorithm 4 to maximize $\widehat{\mathcal{P}}_0$ with all tasks in $\{\mathcal{T}_j\}_{j=1}^K$ serving as auxiliary tasks.

Although this strategy can reduce the computational cost through parameter sharing during inference, it cannot avoid negative transfer as effectively as Algorithm 4, because it does not explicitly model the asymmetric relationships between each target task and the auxiliary tasks.

Algorithm 4 Fork_Merge_v2

Input: initial model parameter θ_0 , total iterations T , interval Δt , number of tasks K , target task index j

Output: final model parameter θ_T^*

- 1: **for** $k = 1$ **to** K **do**
- 2: **if** $k = j$ **then**
- 3: $\lambda_k = 1$
- 4: **else**
- 5: $\lambda_k \leftarrow \text{FORK_MERGE_V0}(\theta_0, \Delta t, \Delta t, k, j)$ ▷ estimate relevance of the k -th task
- 6: **end if**
- 7: **end for**
- 8: sort tasks such that $\lambda_1 \geq \lambda_2 \geq \dots \geq \lambda_K$
- 9: **for** $k = 1$ **to** K **do**
- 10: $\nu^k \leftarrow \sum_{i=1}^k \mathbf{e}_i$ ▷ \mathbf{e}_i is the base vector
- 11: $\bar{\Lambda}_k \leftarrow \lambda_k - \lambda_{k+1}$ ▷ construct $\bar{\Lambda}$
- 12: **end for**
- 13: $\{k_l\}_{l=1}^L \leftarrow$ indexes of the largest $L = \lceil \log_2(K) \rceil$ values in $\bar{\Lambda}$ ▷ prune the forking branches
- 14: $\theta_T^* \leftarrow \text{FORK_MERGE_V1}(\theta_0, \{\nu_{k_l}\}_{l=1}^L, T, \Delta t, K, j)$

B. Analysis Details

In this section, we provide the implementation details of our analysis experiment in Section 2.

We use task **P** and **Q** in DomainNet (Peng et al., 2019) as examples of WNT and SNT, and other tasks (**R, S, I, C**) in DomainNet as auxiliary tasks. Details of these tasks are summarized in Table 6. We use ResNet-18 (He et al., 2016) pre-trained on ImageNet (Deng et al., 2009) for all experiments.

B.1. Effect of Gradients Conflicts

First, we optimize the model on the target task for $T = 25\text{K}$ iterations to obtain θ_T . We adopt mini-batch SGD with momentum of 0.9 and batch size of 48, and the initial learning rate is set as 0.01 with cosine annealing strategy (Loshchilov & Hutter, 2017).

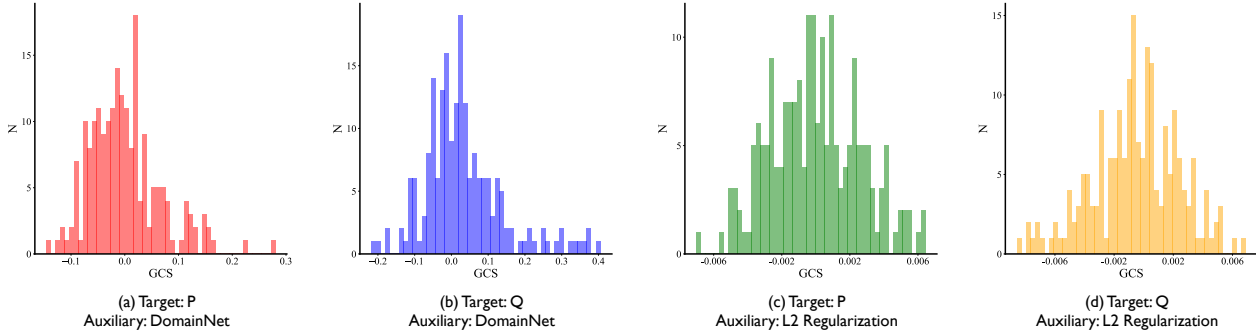


Figure 10. The distribution of GCS.

We repeatedly sample a mini-batch of data and estimate the gradients for the target and auxiliary task \mathbf{g}_{tgt} and \mathbf{g}_{aux} . Figure 10 plots the distribution of GCS between \mathbf{g}_{tgt} and \mathbf{g}_{aux} . We find that the gradients of different tasks are nearly orthogonal ($\cos \phi_{ij} \approx 0$) in most cases, and highly consistent gradients or severely conflicting gradients are both relatively rare.

Then, we optimize the same θ_T with one-step multi-task gradient descent estimated from different data to obtain different θ_{T+1} ,

$$\theta_{T+1}(\lambda) = \theta_T - \eta(\mathbf{g}_{\text{tgt}}(\theta_T) + \lambda \mathbf{g}_{\text{aux}}(\theta_T)), \quad (18)$$

where $\eta = 0.01$ and λ takes values from $\{0, \frac{1}{16}, \frac{1}{8}, \frac{1}{4}, \frac{1}{2}, 1\}$. We evaluate $\theta_{T+1}(\lambda)$ and $\theta_{T+1}(0)$ on the validation set of the

target task to calculate the Transfer Gain from single-step multi-task gradient descent

$$TG(\lambda) = \widehat{\mathcal{P}}(\theta_{T+1}(\lambda)) - \widehat{\mathcal{P}}(\theta_{T+1}(0)). \quad (19)$$

Note that we omit the notation of algorithm \mathcal{A} in Equation (18) and (19) for simplicity. Finally, Figure 1 plots the correlation curve between GCS and TG.

B.2. Effect of Distribution Shift

Interpretation of distribution interpolation. Given the target distribution \mathcal{T}_{tgt} and the auxiliary distribution \mathcal{T}_{aux} , the interpolated distribution of the target and auxiliary task is $\mathcal{T}_{\text{inter}}$,

$$\mathcal{T}_{\text{inter}} \sim (1 - Z)\mathcal{T}_{\text{tgt}} + Z\mathcal{T}_{\text{aux}}, \quad (20)$$

$$Z \sim \text{Bernoulli}\left(\frac{\lambda}{1 + \lambda}\right), \quad (21)$$

where λ is the task-weighting hyper-parameter. Fitting the model on the interpolated distribution $\mathcal{T}_{\text{inter}}$ is equivalent to fitting on the target distribution \mathcal{T}_{tgt} and the auxiliary distribution \mathcal{T}_{aux} simultaneously with multi-task learning.

Qualitative Visualization. We visualize by t-SNE (Van der Maaten & Hinton, 2008) in Figures 3(a) the representations of the training and test data by the model θ_T trained in Section B.1. For better visualization, we only keep the top 10 categories with the highest frequency in DomainNet. To visualize the impact of λ on the interpolated training distribution, we let the frequency of auxiliary task points be proportional to λ . In other words, when the weighing hyper-parameter of the auxiliary task increases, the effect of the auxiliary task on the interpolated distribution will also increase.

Figure 11 provides the t-SNE visualization of training and test distributions when λ takes values from $\{0, \frac{1}{16}, \frac{1}{8}, \frac{1}{4}, \frac{1}{2}, 1\}$. We observe that for WNT tasks, when λ initially increases, the area of training distribution can better cover that of the test distribution. But as λ continues to increase, the distribution shift between the test set and the training set will gradually increase. For SNT tasks, however, the shift between the interpolated training distribution and the test distribution monotonically enlarges as λ increases.

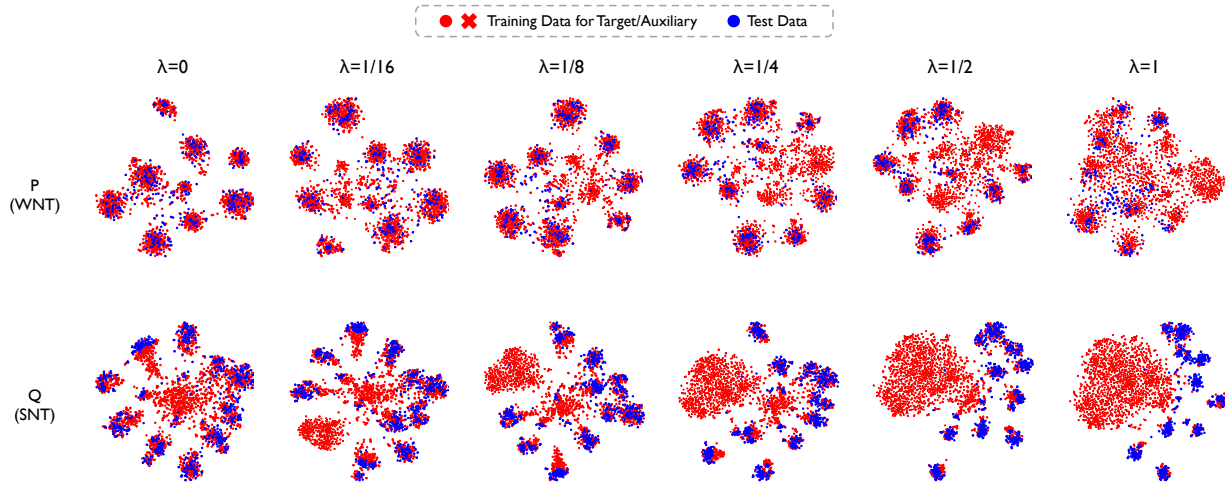


Figure 11. t-SNE visualization of multi-task training distribution and target test distribution.

Quantitative Measure. First, we jointly optimize the model on the target task and auxiliary tasks with different weighting hyper-parameter λ for $T = 25\text{K}$ iterations to obtain $\theta_T(\lambda)$. We adopt the same hyper-parameters as in Section B.1. Then we evaluate $\theta_T(\lambda)$ on the test set of the target tasks and calculate the average confidence on the test set. We can calculate the Confidence Score Discrepancy by Definition 2.5 and the Transfer Gain by

$$TG(\lambda) = \widehat{\mathcal{P}}(\theta_T(\lambda)) - \widehat{\mathcal{P}}(\theta_T(0)). \quad (22)$$

Again, we omit the notation of algorithm \mathcal{A} for simplicity. Finally, we plot the curve between Confidence Score Discrepancy and Transfer Gain under different λ in Figure 3(b).

B.3. Effect of Parameter Distance

It is easier to visualize the Linear Combination Hypothesis Space (LCHS) on a plane when $M = 3$. Thus, each time we will train 3 models and then visualize their LCHS using the ternary heatmaps in Figure 4. The meanings of the vertices of the triangles are listed below:

- **P**: STL model optimized only with target task P;
- **P+R**: MTL model jointly optimized with target task P and auxiliary task R;
- **P+C**: MTL model jointly optimized with target task P and auxiliary task C;
- **Q**: STL model optimized only with target task Q;
- **Q+R**: MTL model jointly optimized with target task Q and auxiliary task R;
- **Q+C**: MTL model jointly optimized with target task Q and auxiliary task C.

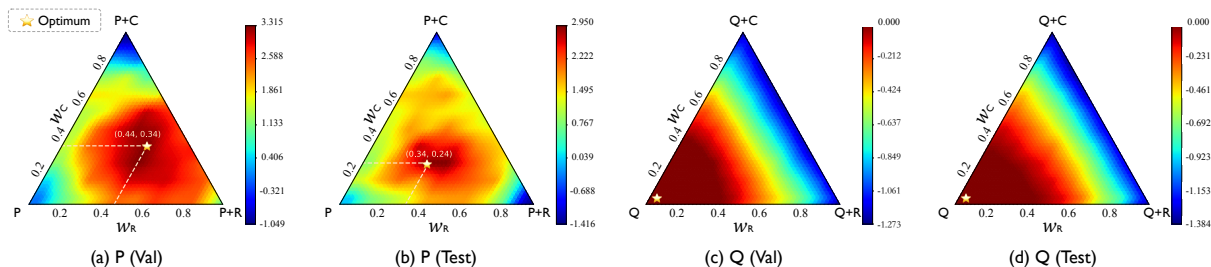


Figure 12. The effect of parameter distance.

After training model **P**, **P+R** and **P+C**, we then enumerate the linear combination coefficients \mathbf{w} from the following sets,

$$\{\mathbf{w} = [1 - w_R - w_C, w_R, w_C]^T | w_R = \frac{m}{10}, w_C = \frac{n}{10}, m, n \in \mathbb{N}, m + n \leq 10, \}, \quad (23)$$

and evaluate each model $\theta = \sum_{m=1}^M w_m \theta_m$ on the validation set. By enumerating all values of \mathbf{w} in Equation (23), we can find the approximate optimal hypothesis. Finally, we interpolate model performance over the continuous space of \mathbf{w}

$$\{\mathbf{w} = [1 - w_R - w_C, w_R, w_C]^T | w_R \geq 0, w_C \geq 0, w_R + w_C \leq 1, \}, \quad (24)$$

to obtain Figure 4 and Figure 12.

C. Experiment Details

C.1. Definition of Δ_m

Following Navon et al. (2022); Lin et al. (2022), we report Δ_m as the performance measure, which is the average per-task performance improvement of method m relative to the STL baseline b . Formally, $\Delta_m = \frac{1}{K} \sum_{k=1}^K (-1)^{z_k} (M_{m,k} - M_{b,k}) / M_{b,k}$ where $M_{b,k}$ and $M_{m,k}$ is the performance of the k -th task obtained by the baseline method b and the compared method m . z_k is set to 0 if a higher value indicates better performance for the k -th task and otherwise 1.

C.2. QM9

Dataset Details. QM9 (Ramakrishnan et al., 2014) is a comprehensive dataset that provides geometric, energetic, electronic, and thermodynamic properties, comprising 134K stable organic molecules represented as graphs. This dataset is under Attribution-NonCommercial-ShareAlike 4.0 International (CC BY-NC-SA 4.0) license.

Experiment Details. We normalize each task target to have zero mean and unit standard deviation since the loss scales vary significantly for different tasks. We use the GNN model from Gilmer et al. (2017), which comprises several concatenated message passing layers and updates the node features based on both node and edge features. Following (Navon et al., 2022), each method is trained for 300 epochs with the Adam optimizer and batch size of 120. We search the initial learning rate in $\{0.0003, 0.001, 0.003\}$ and reduce the learning rate each time the validation metric has stopped improving. In ForkMerge, the parameters are merged every 40 epochs.

C.3. NYU

Experiment Details. We use DeepLabV3+ architecture (Chen et al., 2018a), where a ResNet-50 network (He et al., 2016) pretrained on the ImageNet dataset (Deng et al., 2009) with dilated convolutions is used as a shared encoder among tasks and the Atrous Spatial Pyramid Pooling module is used as task-specific head for each task. Following (Liu et al., 2019a; Yu et al., 2020a), each method is trained for 200 epochs with the Adam optimizer (Kingma & Ba, 2015) and batch size of 8. The initial learning rate is 10^{-4} and halved to 5×10^{-5} after 100 epochs. In ForkMerge, the parameters are merged every 10 epochs. Table 5 presents the full evaluation results of Section 4.2.

Table 5. Performance on NYUv2 dataset (3 tasks in total).

Methods	Segmentation		Depth		Normal					$\Delta_m \uparrow$
	mIoU \uparrow	Pix Acc \uparrow	Abs Err \downarrow	Rel Err \downarrow	Angle Distance		Within t°			
					Mean \downarrow	Median \downarrow	11.25 \uparrow	22.5 \uparrow	30 \uparrow	
STL	51.42	74.14	41.74	17.37	22.82	16.23	36.58	62.75	73.52	-
<i>Methods solving all tasks with a single model</i>										
EW	52.13	74.51	39.03	16.43	24.14	17.62	33.98	59.63	70.93	0.30%
UW	52.51	74.72	39.15	16.56	23.99	17.36	34.46	60.13	71.32	0.63%
DWA	52.10	74.45	39.26	16.57	24.12	17.62	33.88	59.72	71.08	0.07%
RLW	52.88	74.99	39.75	16.67	23.83	17.23	34.76	60.42	71.50	0.66%
MGDA	50.79	73.81	39.19	16.25	23.14	16.46	36.15	62.17	72.97	1.44%
GradNorm	52.25	74.54	39.31	16.37	23.86	17.46	34.13	60.09	71.45	0.56%
PCGrad	51.77	74.72	38.91	16.36	24.31	17.66	33.93	59.43	70.62	0.22%
IMTL	52.24	74.73	39.46	15.92	23.25	16.64	35.86	61.81	72.73	2.10%
GradVac	52.84	74.77	39.48	16.28	24.00	17.49	34.21	59.94	71.26	0.75%
CAGrad	52.04	74.25	39.06	16.30	23.39	16.89	35.35	61.28	72.42	1.41%
NashMTL	51.73	74.10	39.55	16.50	23.21	16.74	35.39	61.80	72.92	1.11%
<i>Methods solving each task with a specific model</i>										
GCS	52.67	74.59	39.72	16.64	24.10	17.56	34.04	59.80	71.04	0.09%
Auto- λ	52.40	74.62	39.25	16.25	23.38	17.20	34.05	61.18	72.05	1.17%
PTFT	52.08	74.86	39.58	16.77	22.98	16.48	36.04	62.27	73.20	1.49%
Ours	54.30	75.78	38.42	16.11	22.41	15.72	37.81	63.89	74.35	4.59%

C.4. DomainNet

Dataset Details. As the original DomainNet (Peng et al., 2019) does not provide a separate validation set, we randomly split 50% data from the test set as the validation set, and use the rest 50% data as the test set. For each task, the proportions of training set, validation set, and test set are approximately 70%/15%/15%. Table 6 summarizes the statistics of this dataset. DomainNet is under Custom (research-only, non-commercial) license.

Table 6. Overview of DomainNet dataset.

Tasks	#Train	#Val	#Test	Description
C	33.5K	7.3K	7.3K	collection of clipart images
R	120.9K	26.0K	26.0K	photos and real world images
S	48.2K	10.5K	10.5K	sketches of specific objects
I	36.0K	7.8K	7.8K	infographic images
P	50.4K	10.9K	10.9K	painting depictions of objects
Q	120.7K	25.9K	25.9K	drawings of game ‘‘Quick Draw’’

Experiment Details. We adopt mini-batch SGD with momentum of 0.9 and batch size of 48. We search the initial learning rate in $\{0.003, 0.01, 0.03\}$ and adopt cosine annealing strategy (Loshchilov & Hutter, 2017) to adjust learning rate during training. We adopt ResNet-101 pretrained on ImageNet as the backbone. Each method is trained for 50K iterations. In ForkMerge, the parameters are merged every 12.5K iterations.

C.5. AliExpress

Dataset Details. AliExpress (Li et al., 2020) is gathered from the real-world traffic logs of AliExpress search system in Taobao and contains more than 100M records in total. We split the first 90% data in the time sequence to be training set and the rest 5% and 5% to be validation set and test set. AliExpress consists of 2 tasks: click-through rate (CTR) and click-through conversion rate (CTCVR), and 4 scenarios: Spain (ES), French (FR), Netherlands (NL), and America (US). Table 7 summarizes the statistics of this dataset. AliExpress is under Attribution-NonCommercial-ShareAlike 4.0 International (CC BY-NC-SA 4.0) license.

Table 7. Overview of AliExpress dataset, where $CTR = \#Click / \#Impression$ and $CTCVR = \#Purchase / \#Impression$.

Statistics	ES	FR	NL	US
#Product	8.7M	7.4M	6M	8M
#Pv	2M	1.7M	1.2M	1.8M
#Impression	31.6M	27.4M	17.7M	27.4M
#Click	841K	535K	382K	450K
#Purchase	19.1K	14.4K	13.8K	10.9K
CTR	2.66%	2.01%	2.16%	1.64%
CTCVR	0.60%	0.54%	0.78%	0.40%

Experiment Details. The architecture of most methods is based on ESMM (Ma et al., 2018b), which consists of a single embedding layer shared by all tasks and multiple independent DNN towers for each task. The embedding dimension for each feature field is 128. Each method is trained for 50 epochs using the Adam optimizer, with the batch size of 2048, learning rate of 10^{-3} and weight decay of 10^{-6} . The number of shared experts for OMoE, MMoE and PLE is 8.

C.6. Analysis on the merging step Δt

Table 8 shows the full evaluation results of ForkMerge on NYUv2 dataset with different Δt . Figure 13 visualizes the results on all 3 tasks, where we use mIoU for semantic segmentation, absolute error for depth estimation, and mean angle distance for surface normal prediction.

Table 8. Performance of ForkMerge on NYUv2 dataset with different Δt .

Δt (Epoch)	Segmentation		Depth		Normal					$\Delta_m \uparrow$
	mIoU \uparrow	Pix Acc \uparrow	Abs Err \downarrow	Rel Err \downarrow	Angle Distance		Within t°			
					Mean \downarrow	Median \downarrow	11.25 \uparrow	22.5 \uparrow	30 \uparrow	
1	52.70	74.65	39.46	16.52	23.08	16.56	35.92	62.04	73.03	1.81%
3	53.45	75.03	38.81	16.18	22.77	15.98	37.31	63.16	73.68	3.48%
10	54.30	75.78	38.42	16.11	22.41	15.72	37.81	63.89	74.35	4.59%
30	54.28	75.90	38.97	16.38	22.13	15.34	38.71	64.52	74.83	4.64%
100	53.84	75.36	39.15	16.57	22.70	15.94	37.45	63.28	73.77	3.25%

C.7. Analysis on task relationships

Following Standley et al. (2020), we use TG to measure pairwise task relationships. Formally, with a light abuse of notations, let $\hat{\mathcal{P}}(\theta_{\mathcal{A}}(\mathcal{T}))$ denote the performance of algorithm \mathcal{A} when training with task \mathcal{T} . Given a pair of tasks $\mathcal{T}_1, \mathcal{T}_2$, the task relationship $\mathcal{T}_1 \rightarrow \mathcal{T}_2$ is calculated as $\hat{\mathcal{P}}(\theta_{\mathcal{A}}(\mathcal{T}_1, \mathcal{T}_2)) - \hat{\mathcal{P}}(\theta_{\mathcal{A}}(\mathcal{T}_2))$. The task relationships in MTL are usually asymmetric, that is, when task \mathcal{T}_1 is helpful to task \mathcal{T}_2 , task \mathcal{T}_2 may be harmful to task \mathcal{T}_1 .

Task relationships in NYUv2 are visualized in Figure 8. We further examine task relationships on DomainNet. Figure 14

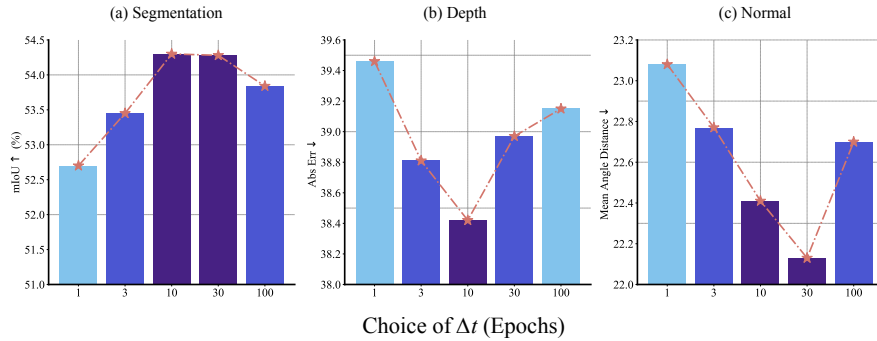


Figure 13. Effect of the merging step Δt on NYUv2.

visualizes the results obtained from (a) EW and (b) ForkMerge, respectively. We can observe that NT is more serious on DomainNet, where 23 of 30 combinations lead to NT when training with EW. In contrast, ForkMerge successfully avoids NT in all 30 combinations. Results support our conclusion that the task relationship in MTL is asymmetric, thus it is better to distinguish the target and the auxiliary task in MTL.

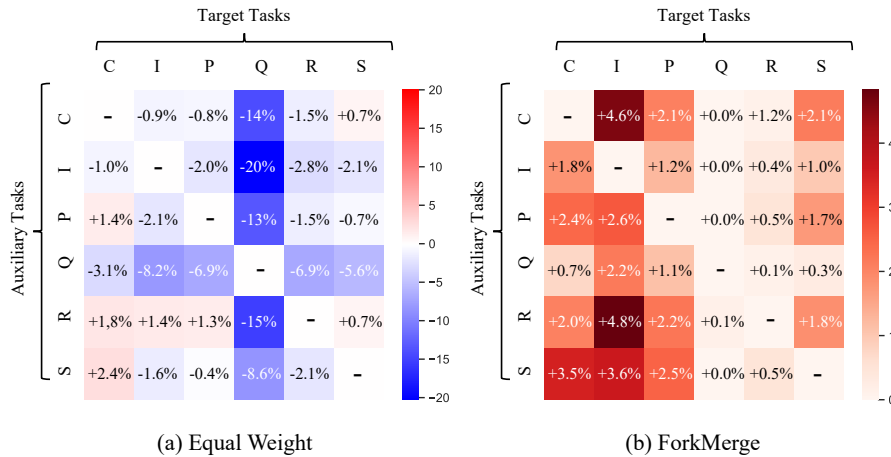


Figure 14. Task relationships on DomainNet. The rows of each matrix represent auxiliary tasks, and the columns represent target tasks. The blue and red cells correspond to negative and positive TG, respectively. Deeper colors indicate stronger impacts.

C.8. Analysis on the importance of different forking branches

Figure 15 plots the full results on all 3 tasks of NYUv2, which is an extension of Figure 7. In this experiment, the number of branches is 3 and the merging step Δt is set to 10 epochs.

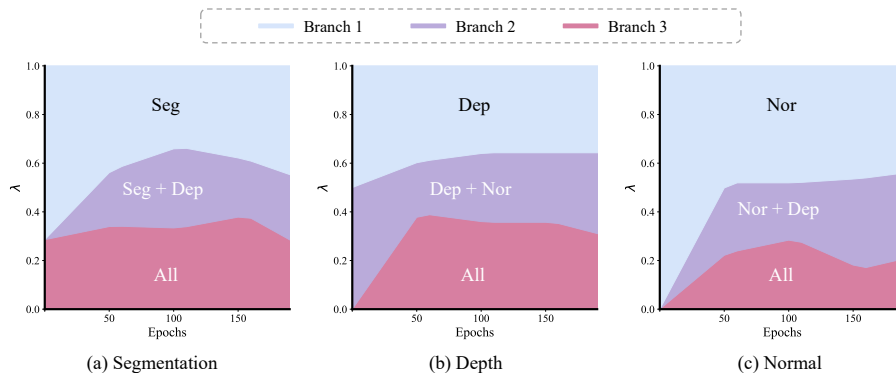


Figure 15. Importance of different forking branches during training on NYUv2.

D. Additional Experiments

D.1. Computation cost of ForkMerge

The computation cost of Algorithm 2 is $\mathcal{O}(K)$ and the computation cost of the pruned version (Algorithm 4) is $\mathcal{O}(\log K)$. Usually, only one model is optimized in most previous multi-task learning methods, yet their computational costs are not necessarily $\mathcal{O}(1)$. Gradient balancing methods, including MGDA (Sener & Koltun, 2018), GradNorm (Chen et al., 2018b), PCGrad (Yu et al., 2020a), IMTL (Liu et al., 2021b), GradVac (Wang et al., 2021), CAGrad (Liu et al., 2021a), NashMTL (Navon et al., 2022), and GCS (Du et al., 2018), require computing gradients of each task, thus leading to $\mathcal{O}(K)$ complexity. In addition, calculating the inner product or norm of the gradients will bring a calculation cost proportional to the number of network parameters. A common practical improvement is to compute gradients of the shared representation (Sener & Koltun, 2018). Yet the speedup is architecture-dependent, and this technique may degrade performance (Navon et al., 2022).

In Figure 16, we also compare the actual training time across these MTL methods on NYUv2. We can observe that even without pruning, ForkMerge still does not require more time than most other MTL methods. And considering the significant performance gains it brings, these additional computational costs are also worth it. Furthermore, our fork and merge mechanism enables extremely easy asynchronous optimization which is not straightforward in previous methods, thus the training time of our method can be reduced to $\mathcal{O}(1)$ when there are multiple GPUs available.

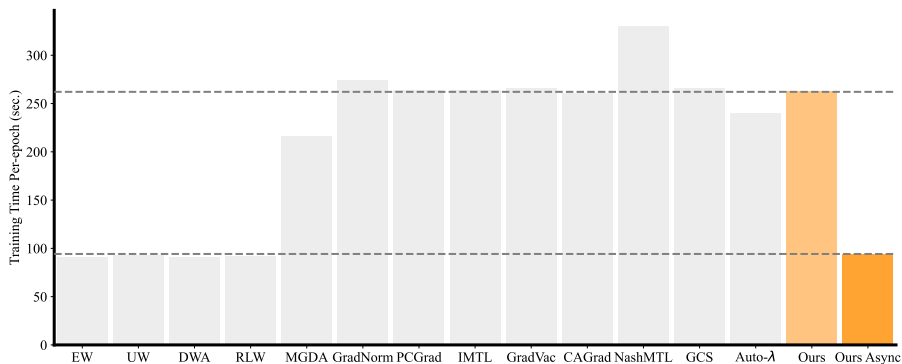


Figure 16. Training speed of different MTL methods on NYUv2 (10 repetitions).

D.2. ForkMerge with multiple target tasks

In Table 9, we provide the results of ForkMerge with multiple target tasks, which is described in Section A.4 and denoted as ForkMerge[‡] on NYUv2. The best previous MTL method solving NYUv2 with a single model is IMTL, with Δ_m of 2.10%. In contrast, our ForkMerge[‡] achieves Δ_m of 2.83%, higher than best result of previous methods.

Table 9. Performance of some method variants on NYUv2 dataset (3 tasks in total).

Methods	Segmentation		Depth		Normal					$\Delta_m \uparrow$
	mIoU \uparrow	Pix Acc \uparrow	Abs Err \downarrow	Rel Err \downarrow	Angle Distance		Within t°			
					Mean \downarrow	Median \downarrow	11.25 \uparrow	22.5 \uparrow	30 \uparrow	
<i>Methods solving all tasks with a single model</i>										
PCGrad	51.77	74.72	38.91	16.36	24.31	17.66	33.93	59.43	70.62	0.22%
GradVac	52.84	74.77	39.48	16.28	24.00	17.49	34.21	59.94	71.26	0.75%
IMTL	52.24	74.73	39.46	15.92	23.25	16.64	35.86	61.81	72.73	2.10%
ForkMerge [‡]	53.65	75.50	38.56	16.08	23.38	16.68	35.70	61.70	72.59	2.83%
<i>Methods solving each tasks with a specific model</i>										
PCGrad [†]	52.70	74.85	39.61	16.24	24.23	17.54	34.06	59.72	70.88	0.54%
GradVac [†]	52.96	74.92	39.60	16.67	23.80	17.16	34.79	60.58	71.67	0.81%
ForkMerge	54.30	75.78	38.42	16.11	22.41	15.72	37.81	63.89	74.35	4.59%

We also provide the results of PCGrad and GradVac with a single target task but multiple auxiliary tasks, which are denoted as PCGrad[†] and GradVac[†]. For each target task, we train a specific model and treat the remaining tasks as auxiliary tasks.

The algorithm-specific implementation details are summarized as follows:

- **PCGrad[†]**: We only calculate gradient conflicts between the target task and auxiliary tasks, but not between auxiliary tasks. When gradient conflicts occur, we always project the gradient of the corresponding auxiliary task. Formally, denote ϕ_{ij} as the angle between the gradient of target task \mathbf{g}_i and the gradient of auxiliary task \mathbf{g}_j . If the cosine similarity is negative, i.e. $\cos \phi_{ij} < 0$, we replace \mathbf{g}_j by its projection onto the normal plane of \mathbf{g}_i : $\mathbf{g}_j = \mathbf{g}_j - \frac{\mathbf{g}_j \cdot \mathbf{g}_i}{\|\mathbf{g}_i\|^2} \mathbf{g}_i$.
- **GradVac[†]**: We only calculate gradient cosine similarity between the target task and auxiliary tasks. Again, we only modify the gradient of the auxiliary task. Formally, denote ϕ_{ij} as the angle between the gradient of target task \mathbf{g}_i and the gradient of auxiliary task \mathbf{g}_j . We update \mathbf{g}_j by $\mathbf{g}_j = \mathbf{g}_j + \frac{\|\mathbf{g}_j\|(\cos \phi_{ij}^T \sqrt{1 - \cos \phi_{ij}^2} - \cos \phi_{ij} \sqrt{1 - (\cos \phi_{ij}^T)^2})}{\|\mathbf{g}_i\| \sqrt{1 - (\cos \phi_{ij}^T)^2}} \mathbf{g}_i$, where $\cos \phi_{ij}^T$ is the exponential moving average of $\cos \phi_{ij}$ during training.

As shown in Table 9, even with a single target task, PCGrad and GradVac still bring slight improvements. This is consistent with our analysis in Section 2.1: Although reducing gradient conflicts can speed up the convergence in optimization, it does not necessarily improve the final generalization performance of the model.

D.3. Comparison with grid searching λ

In Section 2, we observe that adjusting the task-weighting hyper-parameter λ can effectively reduce the negative transfer and promote the positive transfer. [Xin et al. \(2022\)](#) also suggests that sweeping the task weights should be sufficient for full exploration of the Pareto frontier at least for convex setups and observe no improvements in terms of final performance from previous MTL algorithms compared with grid search.

In Figure 17, we compare the performance of all methods with grid search on NYUv2. In grid search, the weighting hyper-parameter for each task takes values from $\{0.3, 1.0, 3.0\}$, and there are 3 tasks in NYUv2, thus there are 27 combinations in total. We find that previous multi-task learning methods simply yield performance trade-off points on the scalarization Pareto front, which has also been observed in previous work ([Xin et al., 2022](#)). In contrast, our proposed ForkMerge yields point far away from the Pareto front and achieves significant improvement over simply optimizing a weighted average of the losses. One possible reason for the gain is that the task weighting in grid search is fixed during training and takes finite values due to the limitation of computing resources while the task weighting in ForkMerge is *dynamic* in time and nearly *continuous* in values, thus can better avoid negative transfer and promote positive transfer.

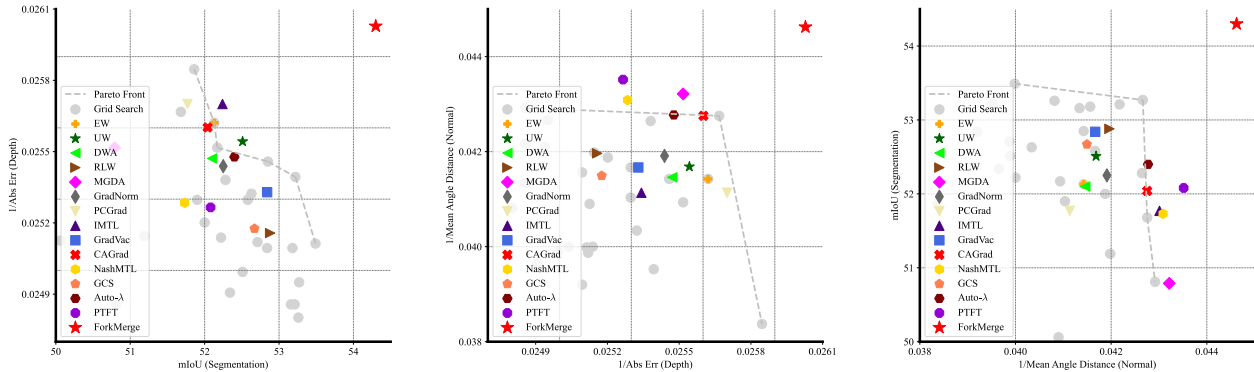


Figure 17. Comparison with grid search on NYUv2. We use mIoU for semantic segmentation, $1/\text{absolute error}$ for depth estimation, and $1/\text{mean angle distance}$ for surface normal prediction. We plot 2D projections of the performance profile for each pair of tasks. Although we plot pairwise projections for visualization, each point in the plots solves all tasks. Top-right is better.

D.4. Convergence and Variance of ForkMerge

Figure 18 plots the validation performance of STL, EW, and ForkMerge throughout the training process on NYUv2. Each curve is obtained by optimizing the same MTL method with 5 different seeds. Compared with single-task learning or

minimizing the average loss across all tasks, ForkMerge not only improves the final generalization but also speeds up the convergence and reduces the fluctuations during training.

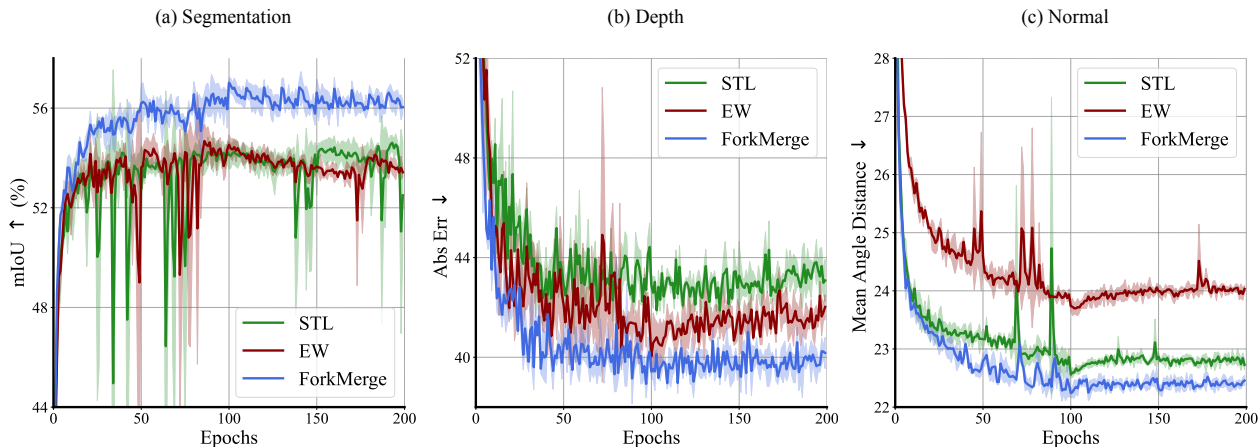


Figure 18. Learning curves comparing different methods on NYUv2. Each curve plots the mean and standard deviation of the validation performance of a method with 5 different random seeds.

D.5. Comparison with larger batch size training

In some sense, the multiple branches in ForkMerge increase the equivalent batch size. And it has been revealed that batch size may have a great effect on the performance of deep models (Goyal et al., 2017; You et al., 2020). To ablate the influence of batch size, we increase the batch size of the Equal Weighting method. As shown in Table 10, the improvement brought by ForkMerge itself is significantly larger than simply increasing the batch size.

Table 10. Comparison of different methods with larger batch size training. ForkMerge[†] is the ForkMerge Algorithm described in Appendix A.4 with a single model for all tasks.

Methods	Batch Size	Segmentation		Depth		Normal					$\Delta_m \uparrow$
		mIoU \uparrow	Pix Acc \uparrow	Abs Err \downarrow	Rel Err \downarrow	Angle Distance		Within t°			
						Mean \downarrow	Median \downarrow	11.25 \uparrow	22.5 \uparrow	30 \uparrow	
EW	8	52.13	74.51	39.03	16.43	24.14	17.62	33.98	59.63	70.93	0.30%
EW	32	51.40	73.99	38.86	16.20	23.99	17.34	34.58	60.08	70.85	0.55%
ForkMerge [†]	8	53.65	75.50	38.56	16.08	23.38	16.68	35.70	61.70	72.59	2.83%

D.6. The influence of pruning

As shown in Table 11, increasing the number of branches L usually improves performance yet the performance gain will gradually saturate as the number of branches increases, thus pruning strategy mentioned in Section 3.2 is an effective strategy in such cases.

Table 11. The effect of branch number on DomainNet.

L	C	I	P	Q	R	S	Avg
<i>Increasing branches improves performance</i>							
1	77.6	41.4	71.8	73.0	84.6	70.2	69.8
2	79.9	42.7	73.5	73.0	85.2	72.0	71.1
3	81.1	44.0	73.7	73.0	85.2	72.7	71.6
<i>Pruning is desired when performance saturates</i>							
4	81.1	44.2	74.4	73.1	85.3	73.0	71.9
6	81.3	44.4	74.7	73.2	85.3	73.4	72.1

D.7. ForkMerge with more multi-task architectures

ForkMerge is complementary to different multi-task architectures. In Tables 12 and 13, we provide a comparison of different multi-task optimization strategies with MTAN (Liu et al., 2019a) and MMoE (Ma et al., 2018a) as architectures, which are widely used in multi-task computer vision tasks and multi-task recommendation tasks respectively.

On these specifically designed multi-task architectures, ForkMerge is still significantly better than other multi-task optimization methods.

Table 12. Performance on NYUv2 dataset by replacing the DeepLabV3+ architecture with the MTAN architecture.

Methods	Segmentation		Depth		Normal					$\Delta_m \uparrow$
	mIoU \uparrow	Pix Acc \uparrow	Abs Err \downarrow	Rel Err \downarrow	Angle Distance		Within t°			
					Mean \downarrow	Median \downarrow	11.25 \uparrow	22.5 \uparrow	30 \uparrow	
STL	52.10	74.42	40.45	16.34	22.35	15.23	38.96	64.56	74.51	3.05%
EW	53.27	75.36	39.37	16.38	23.61	17.00	35.00	61.01	72.07	1.62%
GCS	53.05	74.79	39.50	16.49	24.05	17.49	34.14	59.88	71.13	0.57%
Auto- λ	52.90	75.03	39.67	16.45	22.71	15.60	38.35	64.09	73.92	3.18%
ForkMerge	55.25	76.16	38.45	16.08	21.94	15.22	38.96	65.04	75.33	5.76%

Table 13. Performance on AliExpress dataset by replacing the ESMM architecture with the MMoE architecture.

Methods	CTR				CVCTR				Avg	$\Delta_m \uparrow$
	ES	FR	NL	US	ES	FR	NL	US		
EW	0.7287	0.7244	0.7225	0.7068	0.8874	0.8669	0.8688	0.8742	0.7974	0.11%
GCS	0.7300	0.7190	0.7270	0.7102	0.8857	0.8773	0.8680	0.8740	0.7989	0.29%
Auto- λ	0.7269	0.7273	0.7256	0.7111	0.8827	0.8811	0.8721	0.8726	0.7999	0.42%
ForkMerge	0.7368	0.7349	0.7359	0.7116	0.8942	0.8791	0.8717	0.8840	0.8060	1.20%

E. Limitations

Computation Cost. ForkMerge requires optimizing multiple branches of models simultaneously, which is computationally expensive when there are many branches. To address this, we introduce the pruning strategy to reduce the complexity to $\mathcal{O}(\log(K))$. In practice, we observe that ForkMerge does not require more time than most other MTL methods (see Section D.1) and it is extremely easy to implement the distributed training version of ForkMerge, which can further reduce the time complexity to $\mathcal{O}(1)$ without sacrificing the model performance at all.

Model Capacity. Considering that the task relationships in multi-task learning are often asymmetric, in most of our experiments, ForkMerge solves each task with a specific model to better avoid negative transfer which, however, increases the model capacity in some senses. To tackle this issue, we compare with other MTL methods that solve each task with a specific model, such as Auto- λ (Liu et al., 2022), GCS (Du et al., 2018), Pretrain-Finetune (Liu et al., 2019c), and we also increase the model capacity of existing gradient balancing methods (see Section D.2), yet we find that none of them achieves as good results as ForkMerge. On the other hand, when we decrease the model capacity of ForkMerge, forcing it to solve all tasks within a single model, we observe that ForkMerge still outperforms existing MTL methods (see Section D.2). This indicates that ForkMerge is very effective even without increasing the parameter capacity. But it is still at risk of negative transfer when solving all tasks within a single model. Therefore, a future research direction is how to combine ForkMerge with task grouping methods (Zamir et al., 2018; Standley et al., 2020; Song et al., 2022) to achieve better multi-task learning performance with limited model capacity.